Naval Research Laboratory

Stennis Space Center, MS 39529-5004

NRL/MR/7320--13-9444

Tests of Parameterized Langmuir-Circulation Mixing in the Ocean's Surface Mixed Layer

Paul J. Martin
Erick Rogers
Rick A. Allard
James D. Dykes
Patrick J. Hogan

Ocean Dynamics and Prediction Branch
Oceanography Division

September 30, 2013

REPORT DOCUMENTATION PAGE

Form Approved
OMB No. 0704-0188

1. REPORT DATE *(DD-MM-YYYY)*	**2. REPORT TYPE**	**3. DATES COVERED** *(From - To)*
30-09-2013	Memorandum Report	

4. TITLE AND SUBTITLE

Tests of Parameterized Langmuir-Circulation Mixing in the Ocean's Surface Mixed Layer

5a. CONTRACT NUMBER

5b. GRANT NUMBER

5c. PROGRAM ELEMENT NUMBER
0602435N

6. AUTHOR(S)

Paul J. Martin, Erick Rogers, Rick A. Allard, James D. Dykes, and Patrick J. Hogan

5d. PROJECT NUMBER

5e. TASK NUMBER

5f. WORK UNIT NUMBER
73-6288-02-5

7. PERFORMING ORGANIZATION NAME(S) AND ADDRESS(ES)

Naval Research Laboratory
Oceanography Division
Stennis Space Center, MS 39529-5004

8. PERFORMING ORGANIZATION REPORT NUMBER

NRL/MR/7320--13-9444

9. SPONSORING / MONITORING AGENCY NAME(S) AND ADDRESS(ES)

Office of Naval Research
One Liberty Center
875 North Randolph Street, Suite 1425
Arlington, VA 22203-1995

10. SPONSOR / MONITOR'S ACRONYM(S)

ONR

11. SPONSOR / MONITOR'S REPORT NUMBER(S)

12. DISTRIBUTION / AVAILABILITY STATEMENT

Approved for public release; distribution is unlimited.

13. SUPPLEMENTARY NOTES

14. ABSTRACT

Recent large-eddy simulations (LES) of Langmuir circulation (LC) within the surface mixed layer (SML) of the ocean found that the LCs significantly increase the rate of mixing within the SML. Based on these results, Kantha and Clayson (2004) implemented a parameterization of LC mixing in the Mellor-Yamada Level 2.5 (MYL2.5) turbulence model. This parameterization of LC mixing was implemented in the version of the MYL2.5 turbulence model in the Navy Coastal Ocean Model (NCOM) and tested for (a) a simple mixing case, (b) simulations of the upper-ocean thermal structure at Ocean Weathership Station (OWS) Papa, and (c) simulations of Hurricane Ivan in the Gulf of Mexico. Results of the tests show that the LC-mixing parameterization significantly increases mixing rates in the SML and slightly increases the mixed-layer depth (MLD). The increased mixing rates reduce the shear of the wind-driven current in the SML, which reduces the magnitude of the wind-driven current at the ocean's surface. However, the increased MLD from the LC mixing parameterization is not sufficient to match the observed MLD in the summer at OWS Papa.

15. SUBJECT TERMS

Surface mixed layer — Langmuir circulation
Ocean turbulence — Ocean modeling

16. SECURITY CLASSIFICATION OF:			**17. LIMITATION OF ABSTRACT**	**18. NUMBER OF PAGES**	**19a. NAME OF RESPONSIBLE PERSON**
a. REPORT	**b. ABSTRACT**	**c. THIS PAGE**			Paul Martin
Unclassified Unlimited	Unclassified Unlimited	Unclassified Unlimited	Unclassified Unlimited	50	**19b. TELEPHONE NUMBER** *(include area code)* (228) 688-5447

Standard Form 298 (Rev. 8-98)
Prescribed by ANSI Std. Z39.18

CONTENTS

TESTS OF PARAMETERIZED LANGMUIR-CIRCULATION MIXING IN THE OCEAN'S SURFACE MIXED LAYER

1. INTRODUCTION

Martin (1985, 1986) reported that Mellor-Yamada- (MY-) type turbulence or mixed-layer models (MLMs) (Mellor and Yamada 1974, 1982) tend to underpredict the depth of the surface mixed layer (SML) in tests conducted with data from Ocean Weathership Stations (OWSs) November and Papa. Simulation of the observed response of upper-ocean mixing to hurricanes, e.g., Martin (1982), also suggested that these types of MLMs sometimes do not mix quickly enough. Observations of velocity shear in the SML have suggested that the velocity shear in the SML predicted by MY-type models is too large, which also suggests that the rate of mixing is not strong enough.

There have been a number of efforts to enhance the MY-type MLMs to account for the fact that they frequently do not mix the ocean's SML strongly or deeply enough. Large et al. (1994) proposed a mixing enhancement to account for possible intermittent mixing in the stratified region near the base of the SML by, e.g., enhancement of the local shear by propagating or breaking internal waves. This enhancement provides for a moderate rate of vertical mixing (with a maximum rate of 50 cm^2/s) up to a Richardson number of 0.7, i.e., the additional mixing provided by the enhancement shuts off at a Richardson number of 0.7, rather than a value in the range of 0.20 to 0.25 that is typical of most MY-type MLMs. This mixing enhancement was implemented and tested in their K-Profile Parameterization (KPP) turbulence model by Large et al. (1994) and was found to significantly improve the predicted mixed-layer depth (MLD) relative to observations. The Large et al. (1994) mixing enhancement was also implemented and tested in the Mellor-Yamada Level 2.5 (MYL2.5) MLM by Kantha and Clayson (1994), and they reported a significant improvement in the predicted MLD for several data sets when using this enhancement.

Another enhancement to increase the mixing for MY-type MLMs has been to account for the injection of turbulent kinetic energy (TKE) into the SML by breaking surface waves. This can be parameterized in the MYL2.5 and similar turbulence models by implementing a flux of TKE at the surface from the waves and by setting the turbulent length scale at the surface z_s to account for the surface roughness due to the surface waves.

Craig and Banner (1994) parameterized the surface flux of TKE as αu_*^3, where $\alpha = 100$ and u_* is the water-side surface friction velocity. For their experiments with $u_* = 0.011$ m/s, they used a value of 0.1 m for the surface roughness. However, they note that this choice was somewhat arbitrary and that there is considerable uncertainty in defining the surface roughness for upper-ocean turbulence, i.e., their discussion of estimates from the literature for light to moderate winds includes values from 10^{-4} to more than 1 m. They note that the most popular approach to

Manuscript approved October 10, 2012.

computing z_s is probably the Charnock (1955) formula $z_s = \beta u_*^2/g$, where β is a scaling factor and g is the acceleration of gravity.

The initial finding of using this approach to increasing the mixing in MY-type MLMs is that the additional TKE added near the surface increases the mixing rates near the surface, but that this additional TKE tends to dissipate locally, i.e., near the surface, and does not generally contribute significantly to increasing the vertical mixing deeper in the water column or increasing the depth of the SML (Craig and Banner 1994). However, if the surface roughness is made sufficiently large (i.e., larger than most of the values that were initially tested), the mixing rates throughout the SML are significantly increased and the depth of the SML is increased as well.

This issue was reviewed by Mellor and Blumberg (2004). Based on predicting a sufficiently deep SML at OWS Papa with the MYL2.5 MLM, they recommended values of $\alpha = 100$ for the TKE flux (i.e., the same as the value suggested by Craig and Banner, 1994) and $\beta = 200000$ for the calculation of the surface roughness using the Charnok (1955) formula. Note that this value of β gives a surface roughness of about 2 m in winds of 8 m/s, which is of the order of the surface wave height. Whether such a large surface roughness is appropriate for computing turbulence in the SML is not clear. However, these large values of β do provide a simple way to increase the depth of the SML predicted by MY-type turbulence models, and the predicted deepening of the SML can be adjusted by adjusting the value of β. Note that for the simulations conducted in this report, the value of α was set to 100 and the value of β was set to 40000. This value of β is larger than the smallest values that have been suggested, but is smaller than the largest and is smaller than is needed to significantly affect the MLD.

It has long been thought that Langmuir circulations (LCs) must affect upper-ocean mixing. However, until fairly recently, there have not been quantitative estimates as to what the effects of LCs on upper-ocean mixing are, and so there have been few, if any, attempts to parameterize the effect of LCs on vertical mixing in the SML.

However, improved understanding of LCs and increases in computing power have led to large-eddy simulations (LES) of LCs, which have provided quantitative estimates of the effect of LCs on mixing in the ocean's SML. McWilliams et al. (1997, hereafter referred to as MW97) conducted LES simulations of LCs for a simple, wind-mixing case with an initial MLD of about 33 m and a moderate wind of about 5 m/s. They found that the inclusion of LCs in the LES increased the rate of mixing within the SML by about a factor of 3 and slightly increased the depth of mixing.

Motivated by this result from MW97, Kantha and Clayson (2004, hereafter referred to as KC04) investigated how to implement this increased rate of mixing from the LCs in the widely-used MYL2.5 turbulence model. They added additional shear-production terms to the MYL2.5 model, consisting of the product of the vertical Reynolds stress multiplied by the vertical shear of the Stokes drift current (SDC) from the waves. The additional shear-production terms were added to both the TKE equation and the turbulence length-scale (TLS) equation of the MYL2.5 model.

The effect of these changes on the MYL2.5 turbulence model is generally to increase the TKE and the TLS and the rate of mixing within the SML. For the conditions of the simple, light-wind simulation conducted by MW97, KC04 found that the maximum rate of mixing in the SML was significantly increased and the mixing rates were fairly consistent with the LES results of MW97.

Some properties of the KC04 modification to the MYL2.5 turbulence model are that (1) since it depends on the SDC from the waves, the additional mixing is generally confined to the region of influence of the surface waves in the SML, i.e., the additional mixing does not affect interior or bottom mixed layers unless the water is fairly shallow, and (2) since the additional shear-production terms depend on the product of the vertical momentum flux and the vertical shear of the SDC, and the vertical momentum flux is parameterized as the product of the vertical mixing coefficient and the vertical shear of the ocean model's Eulerian velocity, if there are waves but the winds are light, so that the vertical shear of the model Eulerian velocity is small, the additional shear-production terms will not generate much mixing, i.e., in the presence of waves or swell but weak winds, the additional shear-production terms will generally not cause much mixing. Both of these properties may be desirable for agreement with observations of upper-ocean mixing.

The modifications to the MYL2.5 turbulence model prescribed by KC04 were implemented in the version of the MYL2.5 turbulence model used in the Navy Coastal Ocean Model (NCOM) (Martin 2000; Morey et al. 2003; Barron et al. 2004) and some tests were conducted to see how the prescribed changes perform. The following sections contain a description of the implementation of the KCO4 LC mixing enhancement in the MYL2.5 turbulence model in NCOM (Section 2), a test of the KCO4 LC mixing in NCOM for the simple, light-wind, test case used by MW97 and KC04 (Section 3), a test of the KCO4 LC mixing in NCOM at OWS Papa (Section 4), a test of the KCO4 LC mixing in NCOM for a simulation of Hurricane Ivan in the Gulf of Mexico (Section 5), and a summary (Section 6).

Note that the goal of the tests is to see how much difference the KC04 LC mixing parameterization makes relative to using the basic form of the MYL2.5 turbulence model. In this way we generally follow the testing procedure used by KC04, who chose not make use of the internal-wave mixing enhancement of Large et al. 1994, which they had previously implemented in the MYL2.5 MLM to increase the depth of mixing (Kantha and Clayson 1994). Hence, underprediction of the observed MLD in the tests conducted for this report, e.g., at OWS Papa, is not to be considered a significant issue, since such shortcomings can be remedied by incorporating additional mixing mechanisms, e.g., the internal-wave mixing enhancement of Large et al. 1994 or the large surface roughness suggested by Mellor and Blumberg (2004) or some other mixing mechanism.

2. IMPLEMENTATION OF LC MIXING IN MYL2.5 MLM

The original TKE and TLS equations as implemented in NCOM are

$$\frac{\partial q^2}{\partial t} = -\nabla\cdot(\mathbf{v}q^2) + Qq^2 + \nabla_h(A_H\nabla_h q^2) + \frac{\partial}{\partial z}\left(K_{q_1}\frac{\partial q^2}{\partial z}\right) + 2K_{M_1}\left(\left(\frac{\partial u}{\partial z}\right)^2 + \left(\frac{\partial v}{\partial z}\right)^2\right) + 2K_{H_1}\frac{g}{\rho_o}\frac{\partial\tilde{\rho}}{\partial z} - 2\frac{q^3}{b_1\ell}, \tag{1}$$

$$\frac{\partial q^2\ell}{\partial t} = -\nabla\cdot(\mathbf{v}q^2\ell) + Qq^2\ell + \nabla_h(A_H\nabla_h(q^2\ell)) + \frac{\partial}{\partial z}\left(K_{q_1}\frac{\partial q^2\ell}{\partial z}\right) + E_1\ell K_{M_1}\left(\left(\frac{\partial u}{\partial z}\right)^2 + \left(\frac{\partial v}{\partial z}\right)^2\right) + E_3\ell K_{H_1}\frac{g}{\rho_o}\frac{\partial\tilde{\rho}}{\partial z} - E_2\frac{q^3}{b_1}W, \tag{2}$$

where q is the square root of twice the TKE, ℓ is the turbulent length scale, t is the time, $\mathbf{v}$ is the vector velocity, Q is a volume flux source term, A_H is the horizontal mixing coefficient for the scalar fields, z is the vertical coordinate, K_{q_1} is the vertical diffusion coefficient for q^2 and $q^2\ell$, which is taken to be proportional to K_{M_1} ($K_{q_1} = 0.41K_{M_1}$), K_{M_1} is the vertical mixing coefficient for momentum, u and v are the horizontal components of the velocity, K_{H_1} is the vertical diffusion coefficient for the scalar fields, g is the acceleration of gravity, ρ_o is a reference density for the water, and $\partial\tilde{\rho}/\partial z$ is the vertical gradient of the water density.

W is referred to by Mellor and Yamada (1982) as a "wall proximity" function, which is used to scale ℓ near the surface and bottom. This function is defined by

$$W = 1 + E_4 \left(\frac{\ell}{\kappa L}\right)^2, \tag{3}$$

and in NCOM, L is defined by

$$L^{-1} = (\zeta - z + z_s)^{-1} + (z - H + z_b)^{-1}, \tag{4}$$

where $\kappa = 0.4$ is Von Karman's constant, ζ is the elevation of the free surface, z_s is the surface roughness, z_b is the bottom roughness, and H is the static bottom depth. The symbols b_1, E_1, E_2, E_3, and E_4 are constants and the values of these are specified in Table 1.

Table 1 — Constants for MYL2.5 Turbulence Equations

parameter	*value*
b_1	16.6
E_1	1.8
E_2	1.0
E_3	1.8
E_4	1.33
E_6	7.2

KC04 parameterized the effects of the LC mixing reported by McWilliams et al. (1997) in their LES experiment by adding additional shear production terms to both the TKE and TLS equations in the MYL2.5 turbulence model. The TKE and TLS equations in NCOM with the additional shear production terms used by KC04 are

$$\begin{aligned}\frac{\partial q^2}{\partial t} &= -\nabla\cdot(\mathbf{v}q^2) + Qq^2 + \nabla_h(A_H\nabla_h q^2) + \frac{\partial}{\partial z}\left(K_{q_1}\frac{\partial q^2}{\partial z}\right) \\ &\quad + 2K_{M_1}\left(\left(\frac{\partial u}{\partial z}\right)^2 + \left(\frac{\partial v}{\partial z}\right)^2 + \frac{\partial u}{\partial z}\frac{\partial u_s}{\partial z} + \frac{\partial v}{\partial z}\frac{\partial v_s}{\partial z}\right) + 2K_{H_1}\frac{g}{\rho_o}\frac{\partial\tilde{\rho}}{\partial z} - 2\frac{q^3}{b_1\ell},\end{aligned} \tag{5}$$

$$\begin{aligned}\frac{\partial q^2\ell}{\partial t} &= -\nabla\cdot(\mathbf{v}q^2\ell) + Qq^2\ell + \nabla_h(A_H\nabla_h(q^2\ell)) + \frac{\partial}{\partial z}\left(K_{q_1}\frac{\partial q^2\ell}{\partial z}\right) \\ &\quad + E_1\ell K_{M_1}\left(\left(\frac{\partial u}{\partial z}\right)^2 + \left(\frac{\partial v}{\partial z}\right)^2\right) + E_6\ell K_{M_1}\left(\frac{\partial u}{\partial z}\frac{\partial u_s}{\partial z} + \frac{\partial v}{\partial z}\frac{\partial v_s}{\partial z}\right) \\ &\quad + E_3\ell K_{H_1}\frac{g}{\rho_o}\frac{\partial\tilde{\rho}}{\partial z} - E_2\frac{q^3}{b_1}W,\end{aligned} \tag{6}$$

where u_s and v_s are the horizontal components of the SDC from the waves. An additional constant E_6 is used to scale the Stokes shear production term in the TLS equation and has a value of 7.2 (Table 1). Note that the value of 7.2 for E_6 is different from the value of 4.0 reported in KC04, which was incorrect (Dr. Lakshmi Kantha, personal communication). We found in early testing that the KC04 LC mixing parameterization does not work correctly (i.e., as reported by KC04) with $E_6 = 4.0$.

The original shear-production terms are proportional to the square of the vertical velocity shear; hence, the original shear-production terms are always positive and always act to increase the TKE. The shear-production terms added by KC04 to parameterize the LC mixing contain the vertical shear of the model Eulerian velocity times the vertical shear of the SDC; hence, it is possible for this term to be negative if the two velocity shears are of different sign, which would result in a loss of TKE from this term, rather than a gain. However, in the tests we have conducted so far, this has not seemed to be a large problem, probably because the vertical shear of the model Eulerian current and the SDC usually have the same sign. There will be some further comments about this issue in the test results.

The coupling of NCOM with the output from a wave model requires some additional changes besides enhancing the vertical mixing within the MYL2.5 turbulence model. The SDC is added to NCOM's Coriolis term as described by MW97 and KC04 and many others. This term is referred to as the Stokes-Coriolis term and it affects the downwind transport in the surface wind-driven layer as discussed in MW97 and KC04 and in this report in the next section. The SDC is also used to advect the model fields in NCOM and, to be consistent with this advection, is added to NCOM's continuity equation. Note that the addition of the SDC to NCOM's Coriolis terms affects local, one-dimensional simulations, such as those presented in this report, but the advection by the SDC does not.

Additional wave effects include the surface wave-radiation stress, which is implemented in NCOM similar to the surface wind stress; but since it is generally much smaller than the wind stress, its effect is usually small. Another effect of the waves is the enhancement of bottom drag in shallow water due to the surface-wave orbital motions near the bottom (Grant and Madsen 1979; Soulsby 1995). Both of these additional wave-forcing effects are implemented in NCOM, but these effects are not the focus of this study and will not be discussed further in this report.

3. TEST OF LC MIXING IN MYL2.5 MLM FOR SIMPLE WIND MIXING CASE

MW97 used a simple, wind-mixing test case to look at the effects of LCs on vertical mixing, and KC04 ran the same case to test their parameterization of LC mixing in the MYL2.5 MLM and to compare their results with those of MW97. Hence, we ran the same case to test our implementation of KC04's parameterization of LC mixing in the version of the MYL2.5 MLM in NCOM and to compare with the results of MW97 and KC04.

The initial condition for this test case consists of a SML with a depth of 33 m and a temperature of 13.5 °C and a thermal stratification below the SML of 0.01 °C/m. The salinity is set to a uniform 35 psu both within and below the SML. The initial temperature was chosen to give a thermal expansion coefficient ($1/\rho\partial\rho/\partial T$) of -0.0002 1/°C. The latitude is 43.4 °N to give a value of the Coriolis parameter of 0.0001 1/s, which results in an inertial period of 17.45 h.

The forcing for the test case consists of a surface wind stress of 0.037 Pa, which corresponds to a wind speed of about 5 m/s. MW97 used a small cooling surface heat flux of 5 W/m^2 to speed up the convergence of their LES numerical solution and reduce its run time. We used a linear ramp the length of the inertial period (17.45 h) for the surface wind stress to reduce inertial oscillations and speed the convergence to an approximately steady solution.

The surface wave field for this test case was specified by MY97 as a monochromatic wave of amplitude 0.8 m and wavelength 60 m propagating in the downwind direction. This gives a SDC with a surface value of 0.0679 m/s and an e-folding depth (the inverse of twice the wavenumber, see Appendix A) of 4.78 m, which corresponds to a light swell. This is the SDC used by KCO4 and by us for this test.

NCOM was run for this case in what we refer to as pseudo one-dimensional mode by running the model on a horizontal domain of 2 by 2 grid points (the minimum horizontal grid that NCOM allows) with doubly-periodic lateral boundary conditions. The vertical grid consisted of 40 layers with an upper-layer thickness of 1 m and a uniform stretching to a maximum depth of 200 m; hence, each layer is thicker than the layer above it by about 7%.

With the use of a linear ramp for the surface wind stress, the numerical solution is fairly steady once the ramp ends after 17.45 h. Figure 1 shows profiles of TKE, the vertical mixing coefficient for momentum, and the downwind and crosswind velocity for simulations without and with the parameterization of LC mixing. This figure can be compared with Fig. 2, 3, and 4 in MW97 and with Fig. 1 in KC04.

The TKE in Fig. 1 is roughly doubled by the use of the KC04 LC mixing parameterization, which is qualitatively similar to the result in KC04. Note that the increase in TKE in the upper meter in Fig. 1 is due to the parameterization of the surface flux of TKE from the surface waves.

The maximum value of the vertical mixing coefficient for momentum K_M in Fig. 1 is also roughly doubled, which is qualitatively similar to the result in KC04, i.e., the maximum value of K_M increases from about 200 to 400 cm^2/s, compared with an increase from about 215 to 430 cm^2/s for KC04. For MY97 (their Fig. 3b), the maximum value of K_M increases by about a factor of 3 from about 130 to 380 cm^2/s. However, their maximum value with the LC mixing (380 cm^2/s) is similar to that obtained in our simulation (400 cm^2/s) and by KC04 (430 cm^2/s). The shape of the vertical mixing coefficient profiles in Fig. 1 is more similar to those in MW97 than in KC04 in that the profiles in Fig. 1 and in MW97 have a roughly parabolic shape, whereas the profiles in KC04 reduce fairly abruptly from a maximum value to a value close to zero within a short distance near the base of the SML.

The downwind velocity u in Fig. 1 shows reduced shear with the stronger LC mixing and, as a result, the value of u at the surface is noticeably reduced, which is also shown by KC04 (their Fig. 1) and MW97 (their Fig. 2). Note that the velocity profiles in Fig. 1, in Fig. 2 in MW97, and in Fig. 1 in KC04 are for just the models' Eulerian current and do not include the SDC.

With the inclusion of the SDC in the Coriolis term in the momentum equations, the downwind transport of the Eulerian current is not zero but balances the transport of the SDC, so that the total downwind transport of the Eulerian current plus the SDC is zero. Hence, since the transport

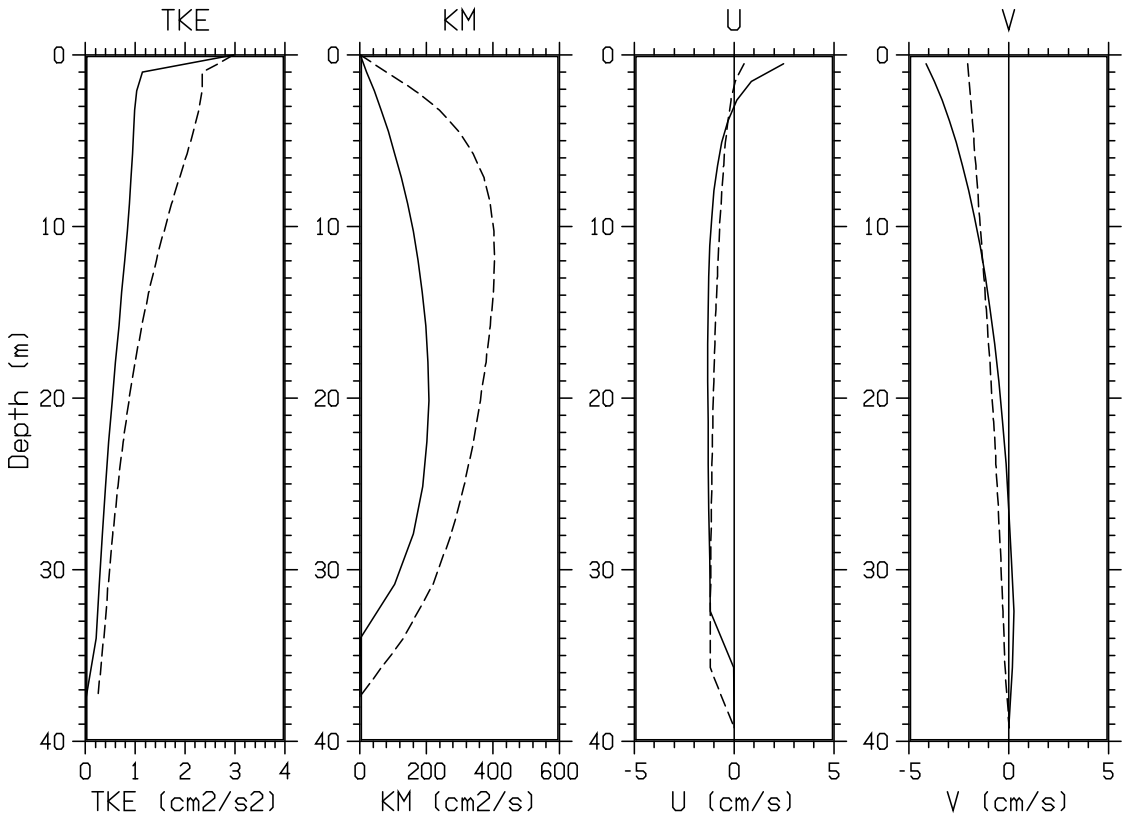

Fig. 1 — Profiles of TKE, vertical mixing rate for momentum, and downwind and crosswind velocity for simulations without (solid line) and with (dashed line) the KC04 LC mixing parameterization for the simple, light-wind, test case.

of the SDC is downwind for this particular test problem, the transport of the downwind component of the Eulerian current in the models is upwind as shown in Fig. 1 and by KC04 and MW97.

A difference of MW97 from the simulation here and in KC04 for the case without the LC mixing is that MW97 drop the SDC from the simulation completely, whereas here and in KC04 the SDC is retained in the calculation of the Coriolis term and is only turned off for the calculation of the vertical mixing in the MYL2.5 turbulence model. Hence, in Fig. 1 and in KC04's Fig. 1, the transport of u for the case without LC mixing is still upwind to balance the downwind transport of the SDC, whereas in MW97, the transport of u for the case without LC mixing is zero (their Fig. 3).

The cross-wind velocity v in Fig. 1 also shows reduced shear with the LC mixing, similar to the cross-wind velocity in MY97 (their Fig. 2), and the surface value of the cross-wind velocity is, as a result, reduced. The transport of the cross-wind velocity must equal the Ekman transport for all of these simulations once they have reached near-equilibrium.

The profiles in Fig. 1 indicate slightly deeper mixing for the case with the LC mixing, i.e., for the case without the LC mixing the MLD increases from the initial value of 33 to 34 m, and for the case with the LC mixing the MLD increases from 33 to 37 m. A deeper MLD with the LC mixing is also indicated in the results of MW97 and KC04.

The velocity profiles in KC04 (their Fig. 1) do not appear completely consistent, since the transports for the cases with and without LC mixing should be the same and they are somewhat different. This may be because the velocity profiles shown by KC04 have not reached equilibrium and there is some residual inertial motion present in the velocity profiles that they show.

In summary, the results obtained for this simple, wind-mixing test case are generally similar to the results reported by KC04 and MW97. The values of the maximum mixing rate for momentum are roughly doubled by including the LC mixing in the results here and in KC04. This is less than the factor of three increase obtained by MW97, but the maximum mixing rate for momentum with the LC mixing obtained here of 400 cm^2/s is similar to that obtained by KC04 and MW97 with the LC mixing. The approximately parabolic shape of the eddy coefficient mixing profiles obtained here with NCOM are roughly similar to the shape of the eddy coefficient profiles obtained by MW97, but are somewhat different from the shape of the profiles in KC04.

4. TEST OF LC MIXING IN MYL2.5 MLM AT OWS PAPA

OWS Papa was located in the northeast Pacific at 145 °W, 50 °N. The availability of long time series of meteorological and ocean subsurface measurements at Papa, and the fact that the effects of advection on the heat budget tend to be small in this area, have long made Papa a popular location to test and evaluate upper-ocean MLMs (Denman and Miyake 1973; Mellor and Durbin 1975; Martin 1985; Martin 1986; Gaspar 1988; Large et al. 1994; Kantha and Clayson 1994; Large 1996).

Simulations were conducted at OWS Papa for the year 1961 using NCOM run in pseudo one-dimensional mode and using the MYL2.5 turbulence model both with and without the LC mixing parameterization of KC04 (i.e., similar to the simulations discussed in the previous section). Hourly

surface wind stresses and heat fluxes were computed from the 3-hourly surface marine observations at Papa using fairly standard formulas as discussed in Martin (1985, 1986).

Note that all the heat fluxes were pre-computed using the surface marine observations from Papa, i.e., the NCOM-predicted SST was not used in the calculation of any of the heat fluxes. The mean computed heat fluxes for the year were 105 W/m^2 for the solar radiation, -88 W/m^2 for the surface heat loss due to the net longwave and latent and sensible heat fluxes, and 18 W/m^2 for the net heat flux. These pre-computed heat fluxes are fairly consistent with the seasonal changes in the observed upper-ocean heat content at Papa during the spring and summer of 1961 (Martin et al. 2012).

Solar extinction was taken to be Jerlov Type II (Jerlov 1968) and the ambient/background viscosity and diffusivity below the SML were taken to be 0.02 cm^2/s. A linear damping term in the momentum equations with a damping time scale of 10 d was used to provide some damping of the inertial oscillations, since the normal horizontal and vertical dissipation of these motions cannot be accounted for in a one-dimensional simulation such as is being conducted here.

The initial condition for the simulations at Papa was a temperature profile from the bathythermograph (BT) observations at Papa for 1 January 1961, and a climatological salinity profile for the location of Papa for the beginning of January from the Levitus (1982) climatology. The salinity profiles at Papa feature a strong halocline between about 100 and 200 m that helps limit the depth of mixing in the winter.

Including the effect of the LC-mixing parameterization of KC04 on the simulation of the SML at Papa requires an estimate of the SDC. Since we don't have wave observations for Papa for 1961, the SDC profile was estimated from the observed surface winds at Papa. There are a number of ways this can be done, and three methods are compared here: (1) compute the SDC from the wind stress using the method used by KC04 for their simulations at OWS Papa, (2) compute the SDC from the wind speed using wave energy spectra time-averaged for different wind speeds using wind and wave data from a NOAA Buoy located in the northeast Pacific about 1100 km east-southeast of Papa, and (3) compute the SDC from the waves predicted by a wave model forced by the observed winds at Papa for 1961.

4.1 Papa Simulations with SDC Computed Using Method of KC04

The method used to estimate the SDC from the surface wind stress by KC04 for their simulations at OWS Papa to test their LC mixing parameterization is to define the surface magnitude of the SDC V_s as a linear function of the friction velocity u_*, i.e., $V_s(0) = 11.8u_*$, and the depth-dependence of the SDC is defined by the wave number k that is characteristic of the peak of the wave-energy spectrum, which is parameterized as $k = 4.05 \times 10^{-6} g/u_*^2$ (see Appendix B). The direction of the SDC is taken to be downwind. This will be referred to as the KC04 SDC. Using this method, hourly profiles of the SDC were computed from the surface wind stress at Papa for 1961 and stored in a file for input to NCOM.

Figure 2 shows results from a simulation of the SML at Papa for 1961 using just the MYL2.5 MLM with no LC mixing enhancement. However, note that the SDC is used in the Coriolis term of the ocean model as discussed in Section 3. In the figure, the results of the simulation (red) are

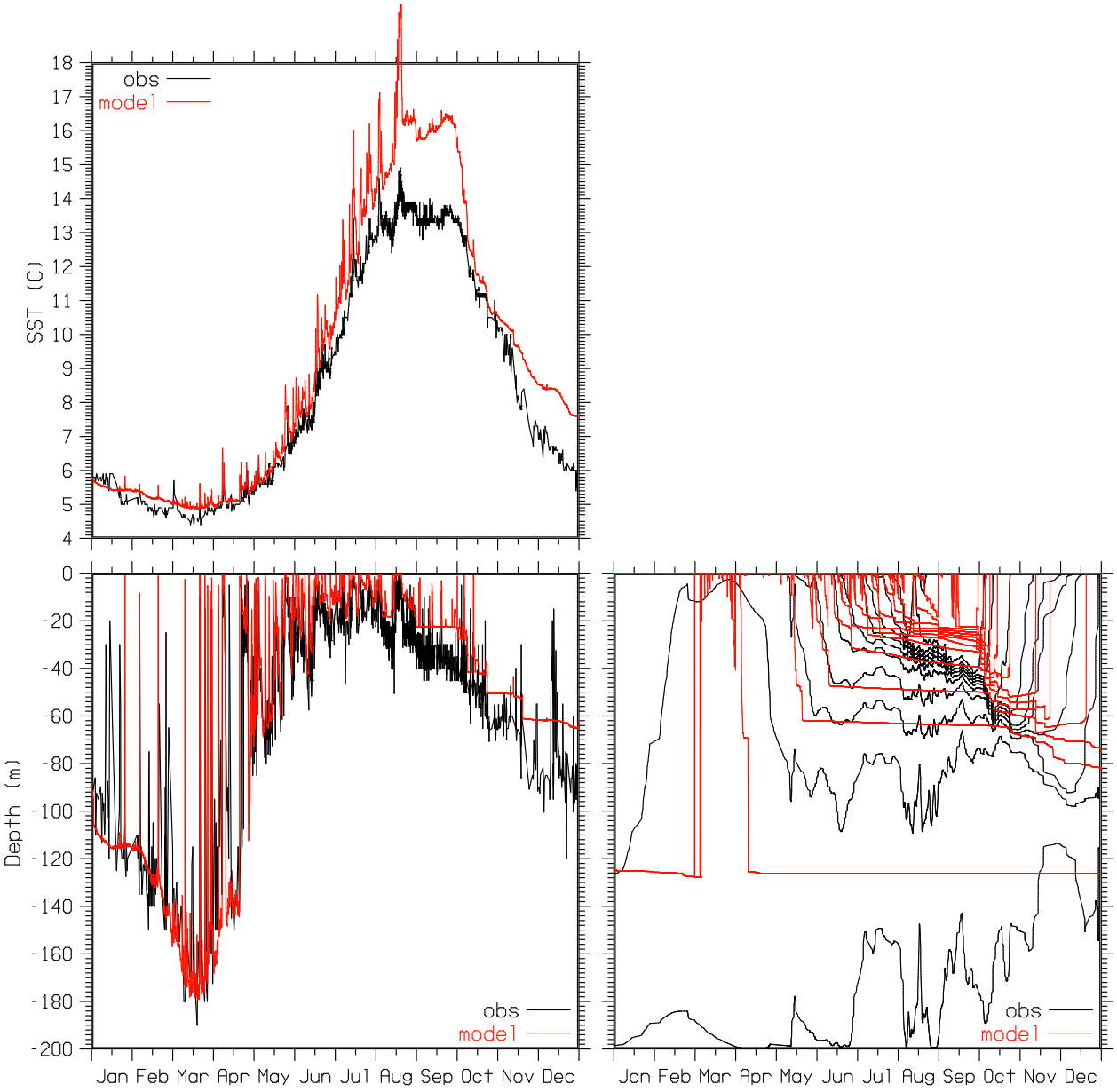

Fig. 2 — SST, MLD, and ISODs at OWS Papa for 1961: observed (black), simulated with KC04 SDC, but without the KC04 LC mixing enhancement (red). ISODs are temporally filtered.

compared with the observations at Papa (black). The MLD shown in the figure is the depth at which the temperature becomes 0.2 °C less than the SST.

As in Martin (1985, 1986), the SST is too high in summer and, consistent with this, the MLD and ISODs are too shallow. In Fig. 2, the summer SST is about 2.5 °C too high and the MLD and ISODs are 10 to 20 m too shallow in August and September. The situation in Fig. 2 is a bit worse than in Martin (1985, 1986) because, for this simulation, the net surface heat flux has been set slightly higher to provide more net heating and better agreement with the observed upper-ocean heat content at Papa in the summer (Martin et al. 2012).

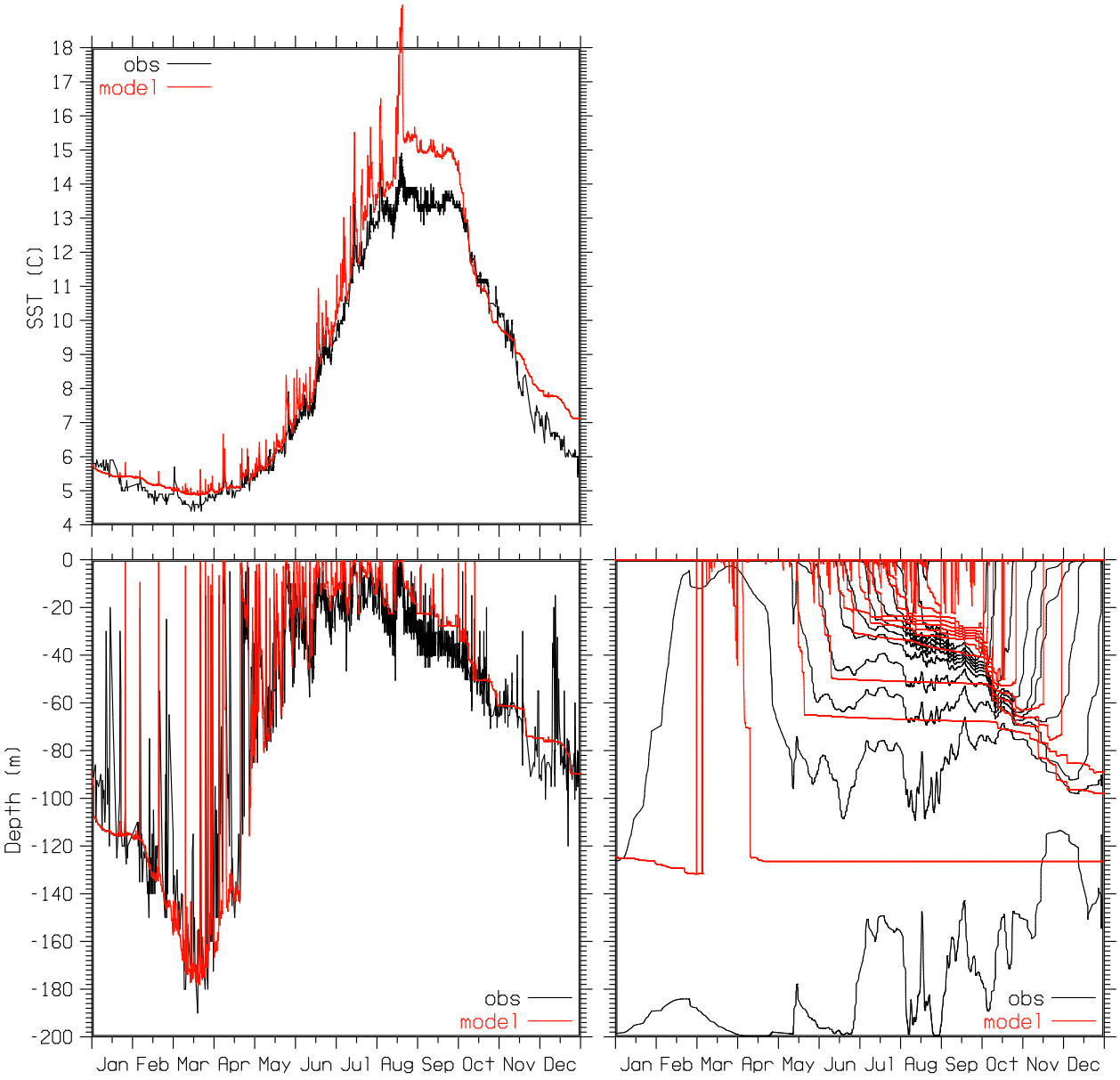

Fig. 3 — SST, MLD, and ISODs at OWS Papa for 1961: observed (black), simulated with KC04 SDC and with the KC04 LC mixing enhancement (red). ISODs are temporally filtered.

Figure 3 shows results from a simulation of the upper-ocean thermal structure at Papa using the MYL2.5 MLM with the KC04 SDC and with the KC04 LC mixing enhancement. Figure 3 shows that the simulation is improved relative to the observations, but the SST is still about 1.6 °C too high in August and September and, consistent with this, the MLD and ISODs are 10 to 15 m too shallow. Hence, the inclusion of the KC04 LC mixing increases the predicted MLD, but the increase does not seem sufficient to account for the observed MLD at Papa in the summer.

Figure 4 shows hourly values of the ratio of the maximum value of the vertical mixing coefficients K_M in the SML for the Papa simulations with and without the KC04 LC mixing enhancement. Plots of the ratio of both unfiltered and temporally filtered K_M values are shown.

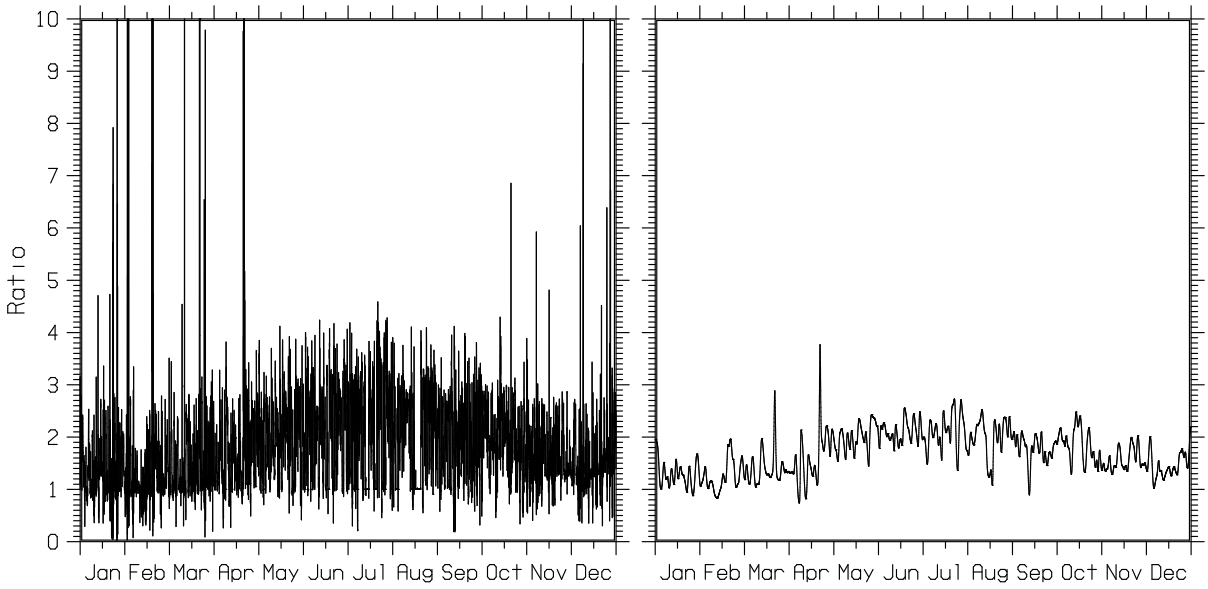

Fig. 4 — Hourly values of the ratio of the maximum value of the vertical mixing coefficients K_M in the SML for Papa simulations with and without the KC04 LC mixing enhancement. The SDC for both of the simulations is computed using the method of KC04. The left plot shows the ratio of unfiltered K_M values and the right plot shows the ratio of temporally filtered K_M values.

The unfiltered plot shows that the range of the ratio of the K_M values is usually between about 0.5 and 3.5, with occasional lower and higher values. Values less than one indicate that the maximum value of K_M for the simulation with the KC04 LC mixing enhancement is lower than that for the simulation without the mixing enhancement. This may sometimes be occurring when the vertical shear of the ocean model's Eulerian velocity and the SDC are of different sign, so that the product of the two makes a negative contribution to the total shear production of TKE.

The plot of the ratio of the temporally filtered K_M values shows a range between about 1.0 and 2.7. The ratio is smaller in the fall and winter when free convection, due mainly to surface cooling, plays a larger role in the vertical mixing, and is larger in the spring and summer when forced convection due to wind forcing and the resulting shear production of TKE plays a larger role. The mean value of the ratio in the spring and summer is about 1.9.

Figure 5 shows hourly values of the magnitude of the surface current for the Papa simulations without and with the KCO4 LC mixing enhancement (note that these time series have been temporally filtered). The mean value of the magnitude of the surface current is reduced about 15% when the KC04 LC mixing enhancement is used. This is somewhat less than the reduction of the surface current by the KC04 LC mixing enhancement shown in Fig. 1. This is because of the frequent occurrence of inertial oscillations in the Papa simulations, which tend to be fairly uniform with depth in the SML and are not significantly affected by the strength of the vertical mixing, whereas for the velocity profiles in Fig. 1 the inertial oscillations were suppressed (by turning on the wind forcing gradually using a linear ramp over one inertial period).

4.2 Papa Simulations with SDC Computed From Buoy Wave Spectra

Nine years of wind and wave data from NOAA Buoy 46005 in the northeast Pacific were used to compute average wave spectra within 1-m/s-wide, wind-speed bins. These average wave spectra were then used to compute hourly SDC profiles at OWS Papa for 1961 based on the hourly wind speed at Papa. The details of this calculation can be found in Appendix C. Buoy 46005 is located at 131.001 °W, 46.100 °N, which is about 1100 km ESE of the location of OWS Papa. Hence, the wind and wave conditions in the area of the buoy should be roughly similar to those near OWS Papa. This calculation of the SDC at Papa will be referred to as the Buoy Wave Spectra (BWS) SDC.

Figure 6 shows results from a simulation of the upper-ocean thermal structure at Papa for 1961 with the BWS SDC, but without the KC04 LC mixing enhancement. Figure 6 shows results similar to Fig. 2, which used the KC04 SDC. The predicted SST is about 3 °C too high in August and September and the predicted MLD at this time is about 10 to 20 m too shallow.

Figure 7 shows results from a simulation of the upper-ocean thermal structure at Papa with the BWS SDC and with the KC04 LC mixing enhancement. The predicted SST and MLD are slightly improved relative to Fig.6, but in August and September, the SST is still about 2 °C too high and the predicted MLD is 10 to 15 m too shallow. The improvement is slightly less than for the case with the KC04 SDC in the previous section. This is because the BWS SDC is generally slightly smaller than the KC04 SDC and provides a smaller enhancement to the vertical mixing.

Figure 8 shows hourly values of the ratio of the maximum value of the vertical mixing coefficients K_M in the SML for the Papa simulations with and without the KC04 LC mixing enhancement.

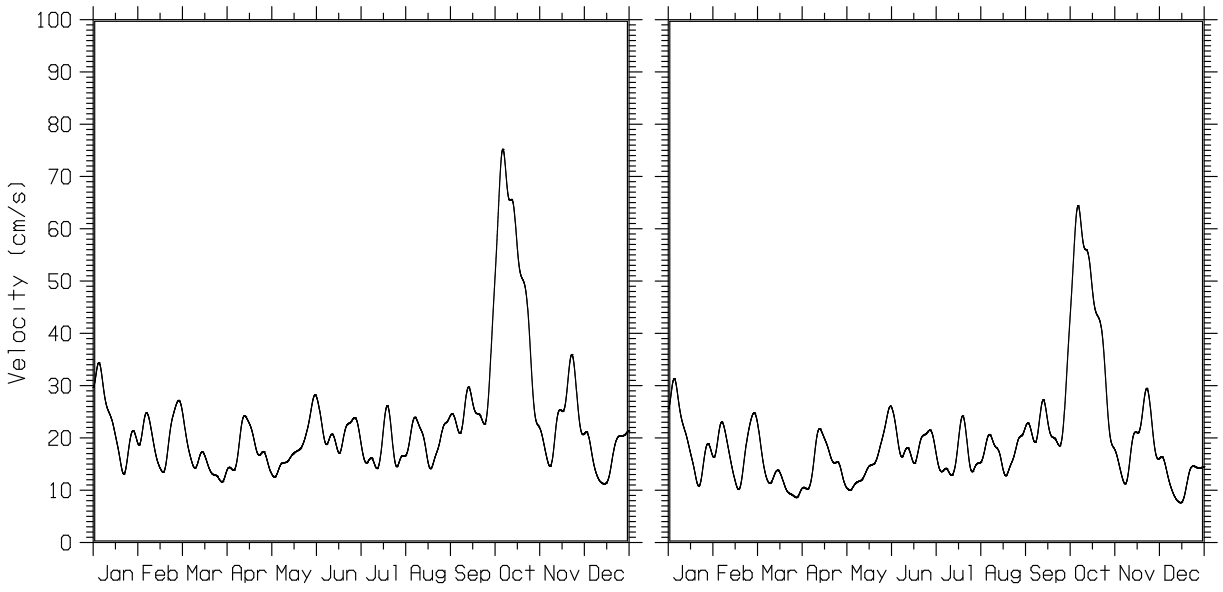

Fig. 5 — Surface current magnitude for simulation without the KC04 LC mixing enhancement (left) and with the KC04 mixing enhancement (right), both plots are strongly temporally filtered.

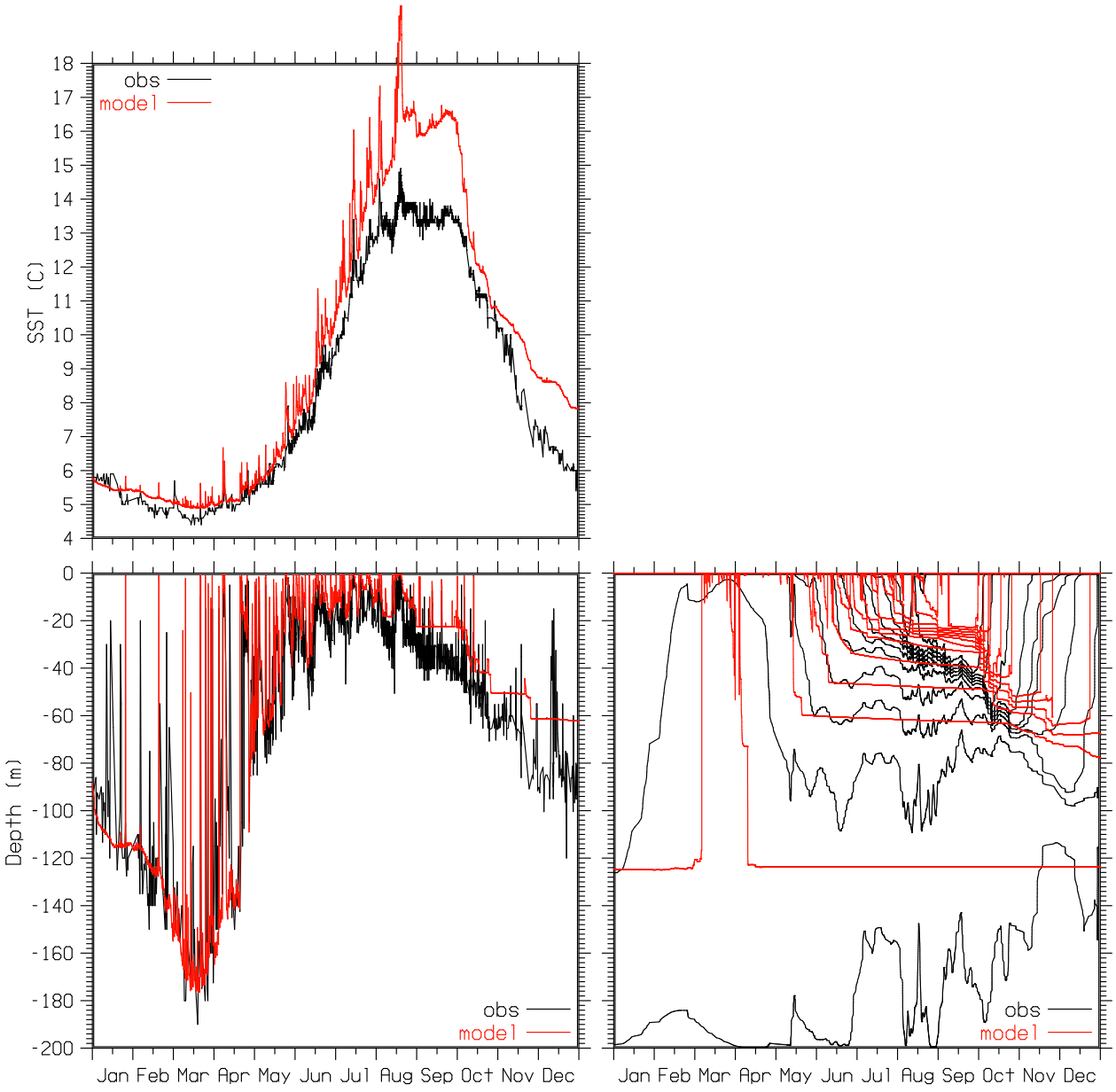

Fig. 6 — SST, MLD, and ISODs at OWS Papa for 1961: observed (black), simulated with the BWS SDC, but without the KC04 LC mixing enhancement (red). ISODs are temporally filtered.

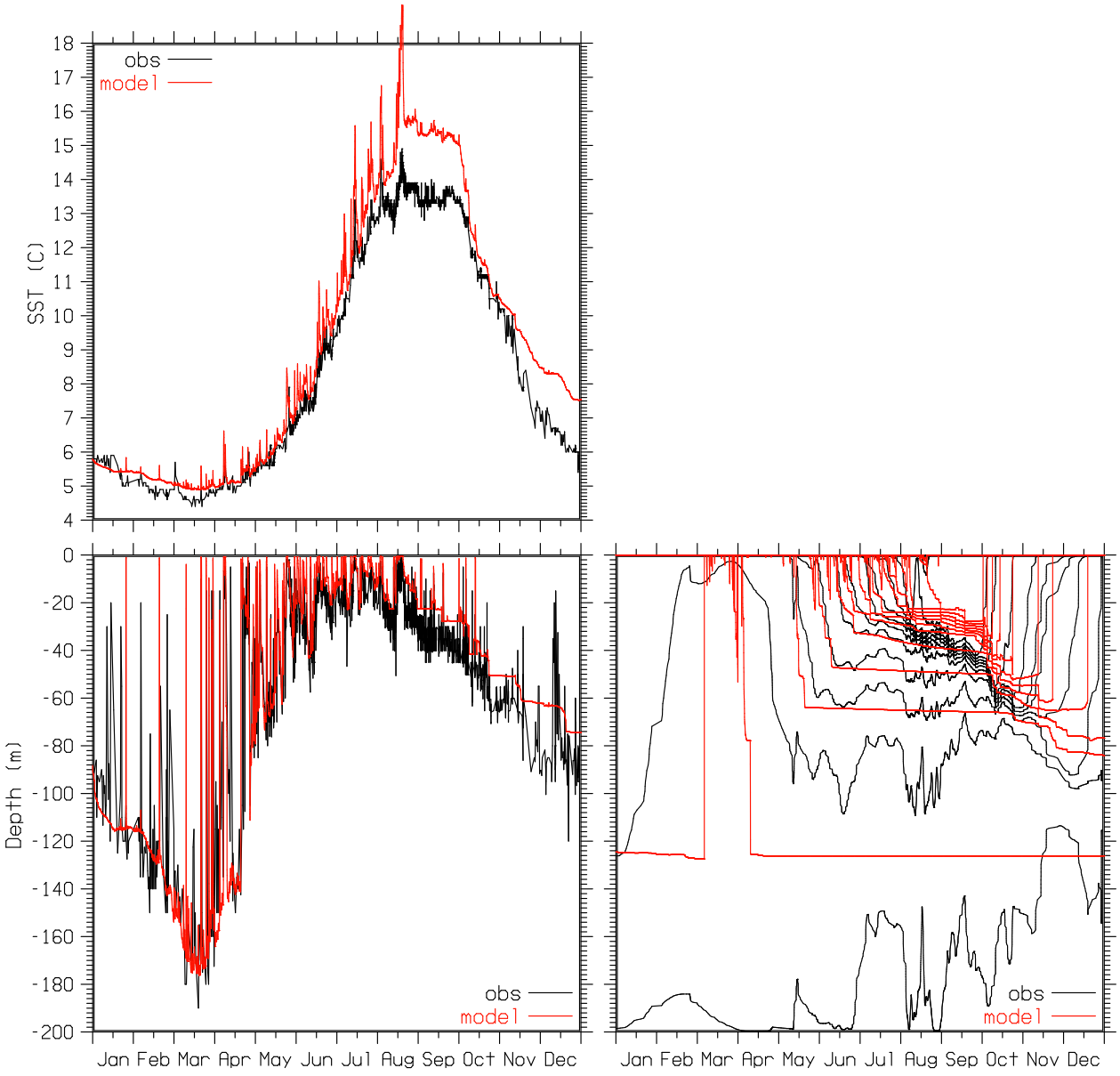

Fig. 7 — SST, MLD, and ISODs at OWS Papa for 1961: observed (black), simulated with the BWS SDC and with the KC04 LC mixing enhancement (red). ISODs are temporally filtered.

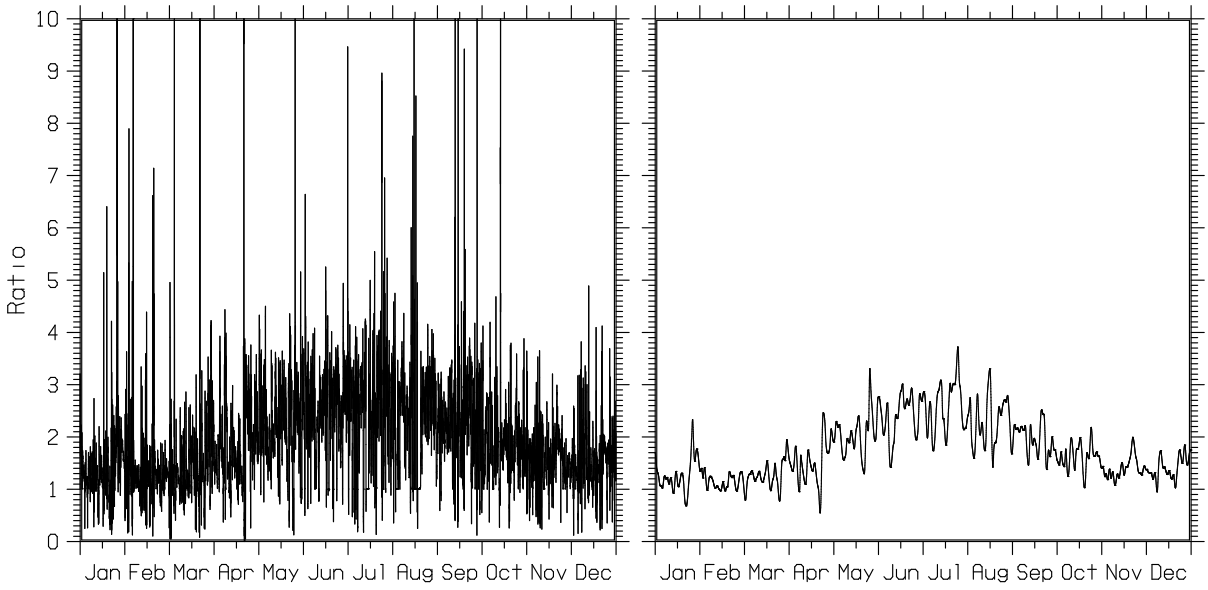

Fig. 8 — Hourly values of the ratio of the maximum value of the vertical mixing coefficients K_M in the SML for Papa simulations with and without the KC04 LC mixing enhancement. The SDC is computed from the BWS. The left plot shows the ratio of unfiltered K_M values and the right plot shows the ratio of temporally filtered K_M values.

Plots of the ratio of both the unfiltered and temporally filtered K_M values are shown. The unfiltered plot shows the range of the ratio of the K_M values is usually between about 1 and 4, with occasional lower and higher values. The plot of the ratio of the temporally filtered K_M values shows a range between about 1.0 and 3.0. As in Fig. 4 with the KC04 SDC, the ratio is larger in the spring and summer when wind-driven forced convection has a more dominant role in the vertical mixing, and the mean value of the K_M ratio in the spring and summer is about 2.1.

Hence, comparing the results for the KC04 LC-enhanced mixing using the BWS and KC04 SDCs, they both increase the mixing rates in the SML in the spring and summer by an average factor of about 2. However, using the BWS SDC results in a slightly smaller increase in the

predicted MLD and a corresponding increase in the predicted SST in the summer because the SDC values are slightly smaller.

4.3 Papa Simulations with SDC Computed from SWAN Wave Model

The SWAN wave model (Booij et al. 1999) was run at OWS Papa for the year 1961 using the observed 10-m winds from Papa, and hourly values of the SDC were computed from the spectral wave output from SWAN and used as input to NCOM. There are several advantages to computing the SDC from a wave model like SWAN over parameterizing the SDC in terms of the current wind stress as was done in the previous two sections. The local wave growth and decay and the direction of the waves can be better accounted for using a wave model. The direction of the waves and the SDC can be somewhat different from the wind direction, depending on the recent history of the wind, and the direction of the SDC can vary with depth since waves of different wavelengths may be propagating in different directions.

There are some issues with regard to running a wave model at a single location, a major one being how to parameterize the wave dissipation. Several wave-dissipation schemes for SWAN were tested by comparison with wave observations from NOAA Buoy 46005, and a dissipation scheme was selected that resulted in the smallest RMS error for the SWAN-predicted significant wave height (this is discussed in Appendix D). A related issue in running a wave model at a single location is that swell propagating from other areas cannot be accounted for.

Figure 9 shows results from a simulation of the upper-ocean thermal structure at Papa with the SWAN SDC, but without the LC mixing enhancement of KC04. In August and September, the predicted SST is about 3 °C too high and the predicted MLD is about 10 to 20 m too shallow.

Figure 10 shows results from a simulation of the upper-ocean thermal structure at Papa with the SWAN SDC with the KC04 LC mixing enhancement. The predicted SST and MLD are slightly improved. In August and September, the SST is still about 2.5 °C too high and the predicted MLD is 10 to 20 m too shallow. The predicted SST in Fig. 10 is slightly higher than for the corresponding runs in the previous two sections in Fig. 3 and 7. The reason for this is that the SWAN SDC is, on average, smaller than both the KC04 and BWS SDCs.

Figure 11 shows hourly values of the ratio of the maximum value of the vertical mixing coefficients K_M in the SML for the Papa simulations with and without the KC04 LC mixing enhancement with the SWAN SDC. Plots of the ratio of both the unfiltered and temporally filtered K_M values are shown. The ratio of the filtered values of K_M in Fig. 11 shows lower values than for the previous simulations, i.e., the general range is from about 0.5 to 2 with a mean during the spring and summer of about 1.4, whereas, for the simulations with the KC04 and BWS SDCs, the mean ratio during the summer is about 2. As in Fig. 4 and 8, the ratio is generally larger in the spring and summer than in the fall and winter.

As was discussed in Section 2, the form of the SDC shear-production terms in the TKE and TLS equations (i.e., in Eq. (5) and (6)) allows for negative values if the vertical gradients of the ocean-model-predicted velocity and the Stokes-drift velocity are of different sign. It is suspected that this is part of the reason that the ratio of K_M values for runs with and without the KC04 mixing enhancement in Fig. 4, 8, and 11 sometimes show values below one. Since the purpose of

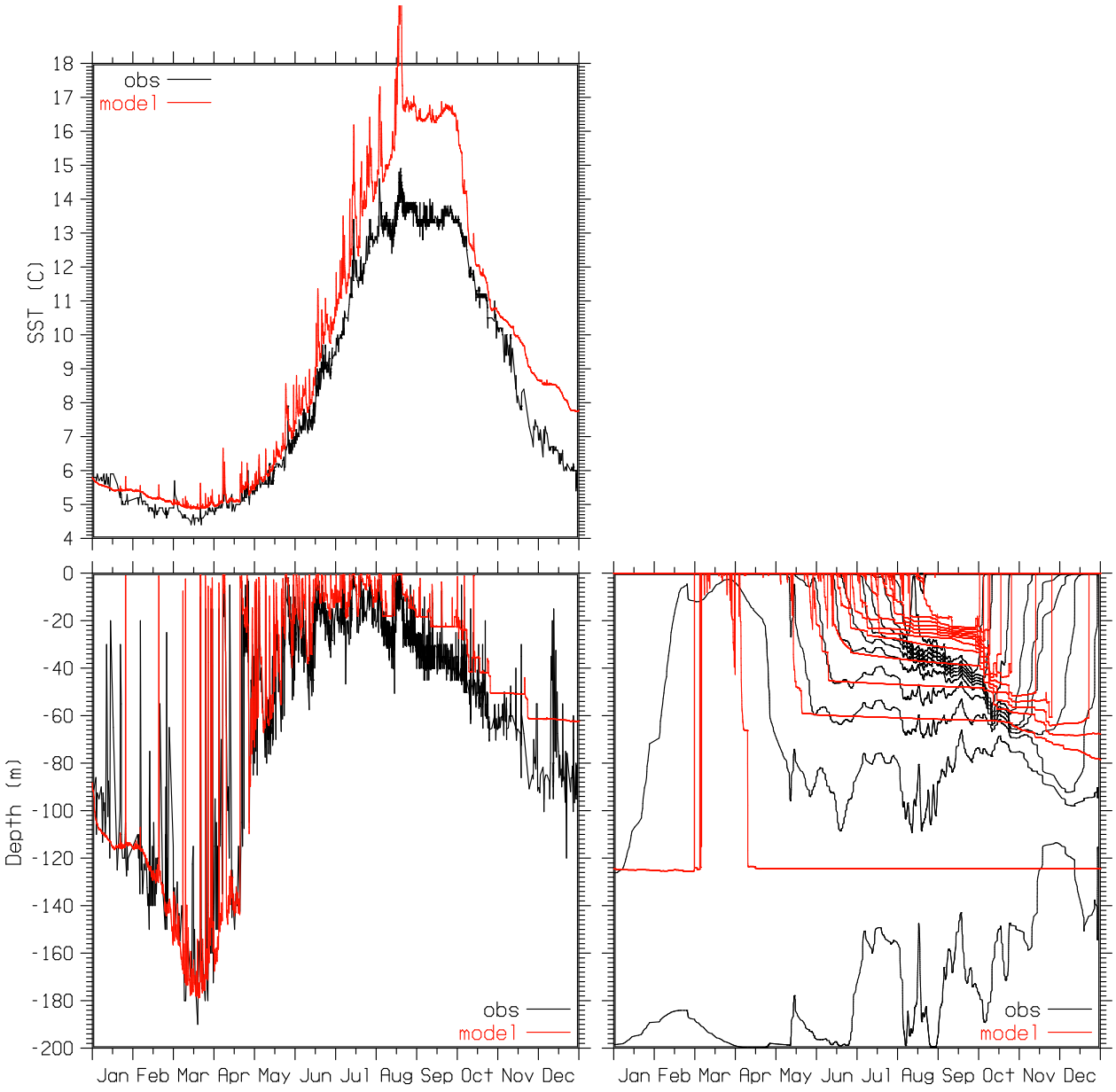

Fig. 9 — SST, MLD, and ISODs at OWS Papa for 1961: observed (black), simulated with the SWAN SDC, but without the KC04 LC mixing enhancement (red). ISODs are temporally filtered.

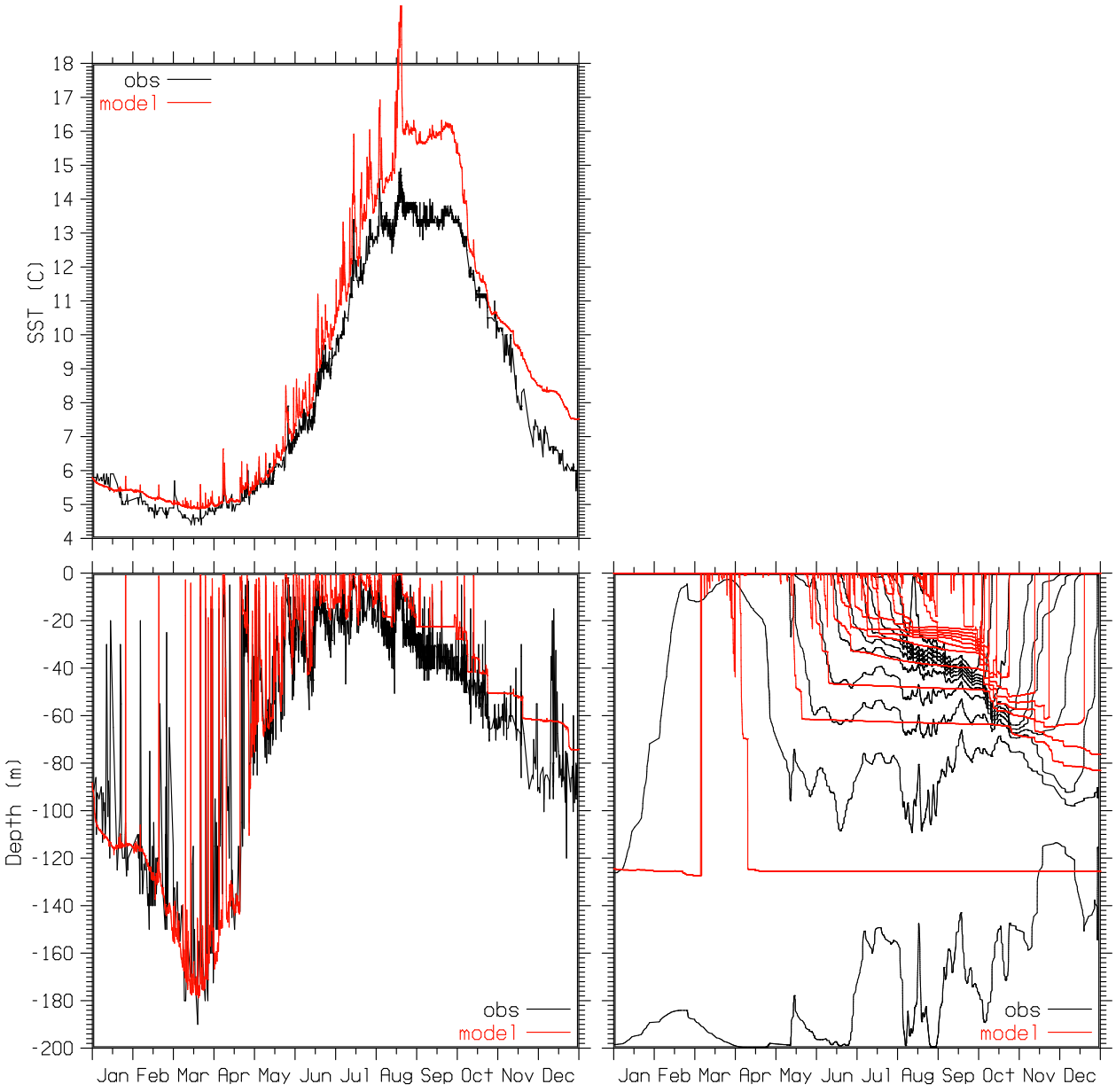

Fig. 10 — SST, MLD, and ISODs at OWS Papa for 1961: observed (black), simulated with the SWAN SDC and with the KC04 LC mixing enhancement (red). ISODs are temporally filtered.

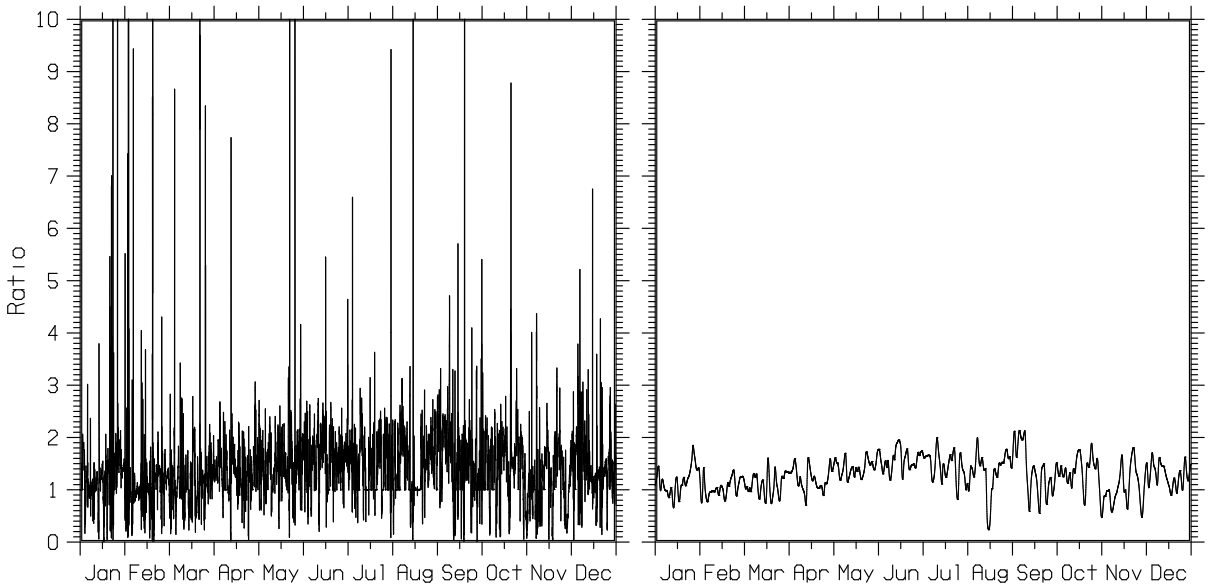

Fig. 11 — Hourly values of the ratio of the maximum value of the vertical mixing coefficients K_M in the SML for Papa simulations with and without the KC04 LC mixing enhancement. The left plot shows the ratio of unfiltered K_M values and the right plot shows the ratio of temporally filtered K_M values. The SDC is from SWAN.

the SDC shear-production terms in the TKE and TLS equations is to parameterize the effects of LC mixing, one might wonder if it is appropriate for these terms to sometimes reduce the rate of mixing in the SML. To investigate the extent to which negative values of the SDC shear-production terms affect the rate of mixing in the SML at Papa, a run was made with the SDC from SWAN with the KC04 mixing enhancement using the absolute value of the SDC shear-production terms to force them to be positive, i.e., the SDC shear-production terms in Eq. (5) and (6) are computed using

$$\mid \frac{\partial u}{\partial z}\frac{\partial u_s}{\partial z} \mid + \mid \frac{\partial v}{\partial z}\frac{\partial v_s}{\partial z} \mid . \tag{7}$$

Figure 12 shows the K_M ratio for runs with and without the KC04 mixing enhancement as in Fig. 11 except that, for the run with the KC04 mixing enhancement, the SDC shear-production terms are forced to be positive. The result is that occurrences of the K_M ratio below one are significantly reduced, especially in the spring and summer. The ratio of the temporally filtered K_M values in Fig. 12 rarely drops below one and the mean value of the K_M ratio in the spring and summer is increased slightly from about 1.4 to 1.6. Since Fig. 12 still shows some values of the K_M ratio below one, it can be said that negative values of the SDC shear-production terms are responsible for a significant fraction of the occurrences of the K_M ratio being below one, but that there are some other causes as well, which may just be due to differences in the temporal evolution of the mixing.

As noted previously, the waves and SDCs predicted by SWAN are frequently not in the same direction as the wind, and the direction of the SDC can vary with depth due to waves of different wavelengths traveling in different directions. To look at the effect of this on the KC04 LC mixing parameterization, a simulation was conducted at Papa with the SDC from SWAN adjusted to always be in the same direction as the surface wind. The results from this simulation (not shown) are similar to the results shown in Fig. 10, i.e., forcing the direction of the SWAN SDC to be downwind did not significantly affect the predicted SST, MLD, ISODs, or the rate of mixing within the SML.

Li et al. (2005) describe a regime diagram for classifying turbulent mixing in the upper ocean. Such a diagram is presented here in Fig. 13 for OWS Papa for 1961 using the SDC from SWAN. The figure shows a scatter plot of hourly values of the Hoenikker number versus the turbulent Langmuir number for Papa for 1961. The Hoenikker number H_o is given by

$$H_o = \frac{4B_0 d_s}{V_s(0)u_*}, \tag{8}$$

where B_0 is the total surface buoyancy flux, d_s is the e-folding depth of the SDC, $V_s(0)$ is the surface value of the SDC, and u_* is the water-side surface friction velocity. The turbulent Langmuir number La_t is given by

$$La_t = (\frac{u_*}{V_s(0)})^{1/2}. \tag{9}$$

The diagram is divided into three regimes according to the type of turbulent mixing: Langmuir, convection, or shear, that dominates within that region. The boundaries of the three regimes were determined by Li et al. (2005) based on LES simulations. The regimes are characterized by

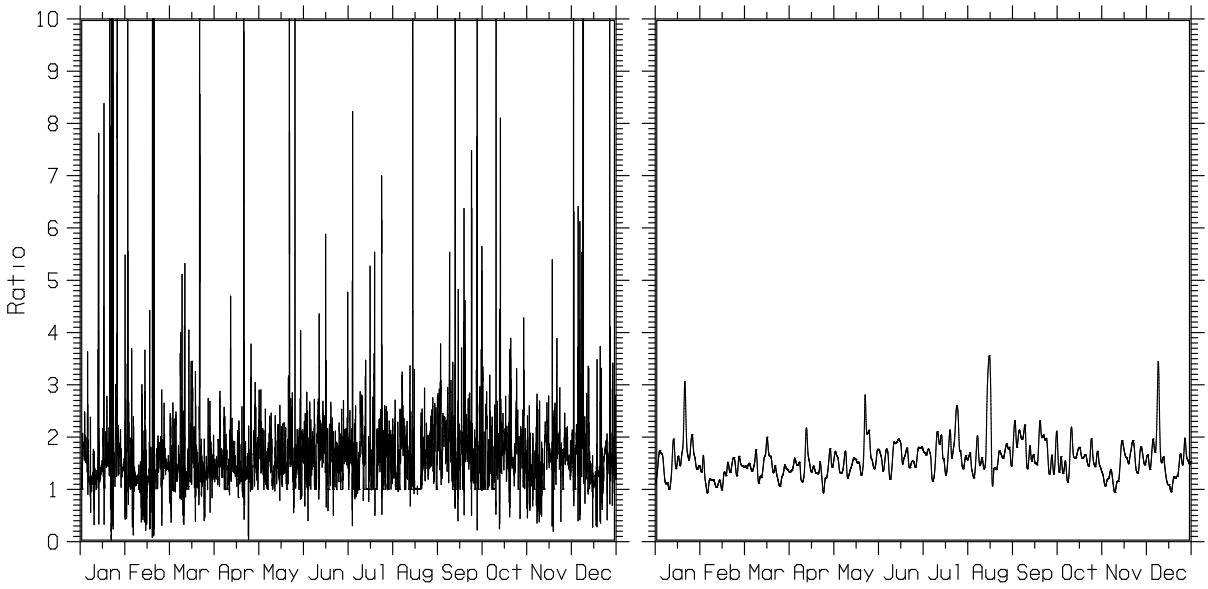

Fig. 12 — Hourly values of the ratio of the maximum value of the vertical mixing coefficients K_M in the SML for Papa simulations with and without the KC04 LC mixing enhancement. The left plot shows the ratio of unfiltered K_M values and the right plot shows the ratio of temporally filtered K_M values. For the simulation with the KC04 mixing enhancement, the SDC shear-production terms are forced to be positive.

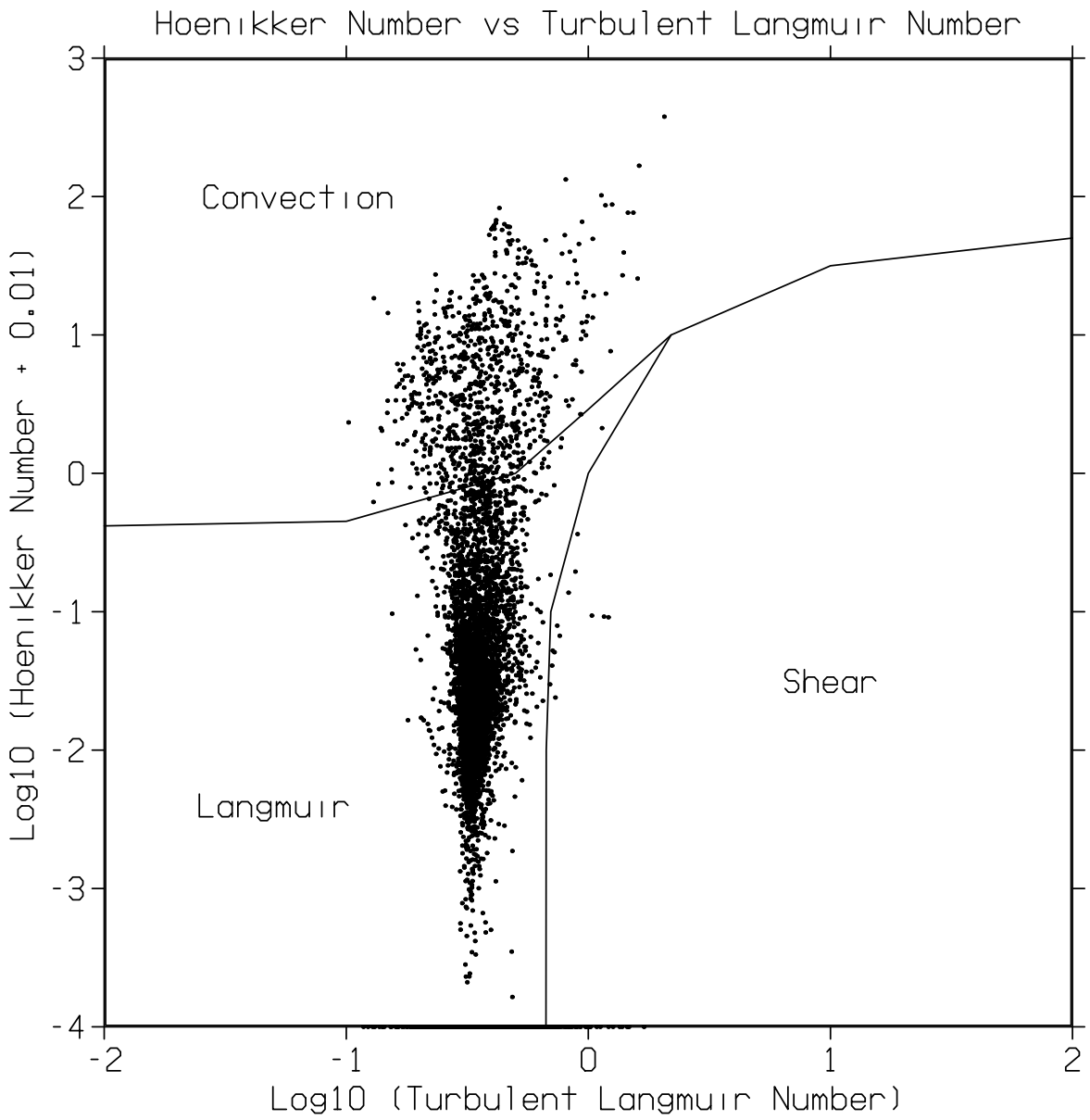

Fig. 13 — Turbulent regime diagram for OWS Papa for 1961 with SDC from SWAN. The points plotted are hourly values of the log10 of the Hoenikker number (with an offset of 0.01) versus the log10 of the turbulent Langmuir number.

the relative magnitudes of the components of the turbulent mixing, with the vertical component dominating in convective mixing, the downwind component dominating in shear mixing, and the cross-wind and vertical components dominating the downwind component in Langmuir mixing.

Figure 13 indicates that the upper-ocean mixing at Papa for 1961 is generally in the Langmuir and convection regimes. Only a few points occur in the shear regime, and these occur close to the boundary between the shear and Langmuir regimes. This is consistent with the finding of Li et al. (2005) that wind mixing in the upper-ocean typically occurs in the Langmuir regime.

Regime diagrams for Papa for 1961 were also calculated (not shown) with the SDC computed using (a) the formulas from KC04 and (b) the mean wave spectra at different wind speeds from Buoy 46005 (as discussed in the previous two sections and in Appendices B and C, respectively). These plots are similar to Fig. 13, though the range of La_t is smaller since the waves and their associated SDC are computed based on the current wind speed. For both of these cases, La_t has a value near 0.3, which is close to the mean value for the SWAN SDC in Fig. 13, and is also close to the value for typical ocean conditions reported by Li et al. (2005).

5. TEST OF LC MIXING IN MYL2.5 MLM FOR HURRICANE IVAN

Simulations were run with NCOM in the Gulf of Mexico (GoM) with wave forcing from SWAN to look at the effect of the KC04 LC mixing enhancement on a simulation of the response of the ocean to Hurricane Ivan in September 2004. Atmospheric forcing was provided from a simulation of Hurricane Ivan with the COAMPS atmospheric model. COAMPS, which stands for Coupled Ocean/Atmosphere Mesoscale Prediction System (Hodur 1997), is currently a coupled atmosphere-ocean-wave modeling system. However, for the simulations conducted here, the atmosphere, ocean, and wave models were run separately. Within the rest of this report, COAMPS will be used to refer to just the COAMPS atmospheric model.

NCOM was run with a horizontal grid resolution of about 4 km. NCOM's vertical grid consisted of 40 layers with a surface layer thickness of 1 m and a smooth stretching to a maximum depth of 5500 m. Initial and boundary conditions for NCOM were provided by the Global NCOM model that is run operationally at the Naval Oceanographic Office at Stennis Space Center, Mississippi (Barron et al. 2004). The COAMPS atmospheric model was run as a triply-nested system with grid resolutions of 81, 27, and 9 km. Initial and boundary conditions for COAMPS were provided by the Navy Operational Global Atmospheric Prediction System (NOGAPS), which is run at the Navy's Fleet Numerical Meteorology and Oceanography Center (FNMOC) in Monterey, California (Rosmond et al. 2002). Hourly surface fields from COAMPS's innermost grid were used to force SWAN and NCOM. These fields include the surface winds for SWAN, and the surface wind stress, surface pressure, solar radiation, net longwave radiation, latent, and sensible heat fluxes, evaporation, and precipitation for NCOM. SWAN was run on the same horizontal grid as NCOM.

Wave fields for forcing NCOM were output hourly from SWAN and include the surface wave radiation stress, the SDC profiles, and the characteristic amplitude, frequency, and direction of the orbital wave motion near the ocean bottom. The wave radiation stress forcing in NCOM is implemented similar to the surface wind stress as a surface stress. In deep water, the wave radiation stress forcing of the ocean is relatively small, i.e., generally less than 10% of the magnitude of the wind stress. The SDC, as noted in Section 2, is used in NCOM's Coriolis and advection terms, in

the continuity equation, and also in the KC04 mixing enhancement. The wave orbital motions near the bottom act to enhance the ocean model's bottom drag in areas where the bottom is sufficiently shallow to feel the orbital wave motions (Grant and Masden 1979; Soulsby 1995). However, the focus here is only on the effect of the KC04 mixing enhancement; hence, the two NCOM simulations that are compared both have full wave forcing from SWAN, and the only difference between them is whether the KC04 mixing enhancement is used or not.

The ocean model simulation was started at 00Z on September 12, 2004. Figure 14 shows the SST and sea-surface velocity (SSV) vectors for the simulation with the KC04 mixing enhancement for 09Z September 15. The surface wind vectors from the COAMPS atmospheric model are also shown. Note that the surface current vectors in Fig. 14 include both the NCOM surface current and the SDC from SWAN. Hurricane Ivan is near the center of the GoM at this time. The hurricane winds generate strong cooling along the hurricane track, with the strongest cooling usually occurring just to the right of the hurricane track (Price 1981).

Figure 15 shows the difference in the SST between the simulation with the KC04 mixing enhancement and without at 09Z September 15, 2004. The simulation with the KC04 mixing enhancement generally shows slightly more cooling of the SST as indicated by the areas of negative temperature difference, but the difference is generally small (less than 0.5 °C). The slightly lower SST for the simulation with the KC04 mixing enhancement indicates slightly deeper mixing, which is consistent with the previous results in Sections 3 and 4.

Figure 16 shows the difference in the SSV between the simulation with the KC04 mixing enhancement and without at 09Z September 15, 2004. The color contours show the difference in the magnitude of the surface current and the black vectors show the vector velocity difference. The fact that the direction of the velocity difference vectors is opposite to the wind direction indicates that the stronger mixing with the KC04 mixing enhancement reduces the wind-driven surface currents. Near the hurricane, the surface currents are reduced by 20 cm/s or more. Some areas show the surface current magnitude with the KC04 mixing enhancement to be larger (as indicated by the color contours in Fig. 16) and this is because the direction of the prevailing currents in these areas is nearly opposite to the wind direction, and so a reduction in the downwind, wind-driven current increases the total current, e.g., on the west side of the hurricane there is an anti-cylonic Loop Current eddy (see Fig. 14).

Figure 17 shows the maximum value of the vertical mixing coefficient K_M in the SML for the simulation with the KC04 mixing enhancement at 09Z September 15, 2004. The K_M values in Fig. 17 were spatially filtered with one pass of a 3x3 box filter. The strongest mixing near the hurricane is occurring on the north and east sides of the eye. A circular area of weak mixing occurs under the eye of the hurricane due to the weak winds there.

The local time for Fig. 17 is about three o'clock in the morning; hence, there is relatively strong night-time convective mixing occurring in some areas, e.g., in the western GoM and the northwest Caribbean. On the afternoon of September 15 (local time), most of this mixing is significantly reduced due to day-time solar heating (not shown). However, the mixing near the hurricane is primarily wind-driven and remains strong through the day and night. Also, the stronger mixing south of and just north of Cuba is partly due to this area being on the warm side of the Loop Current where the SML is generally deeper than on the cold side.

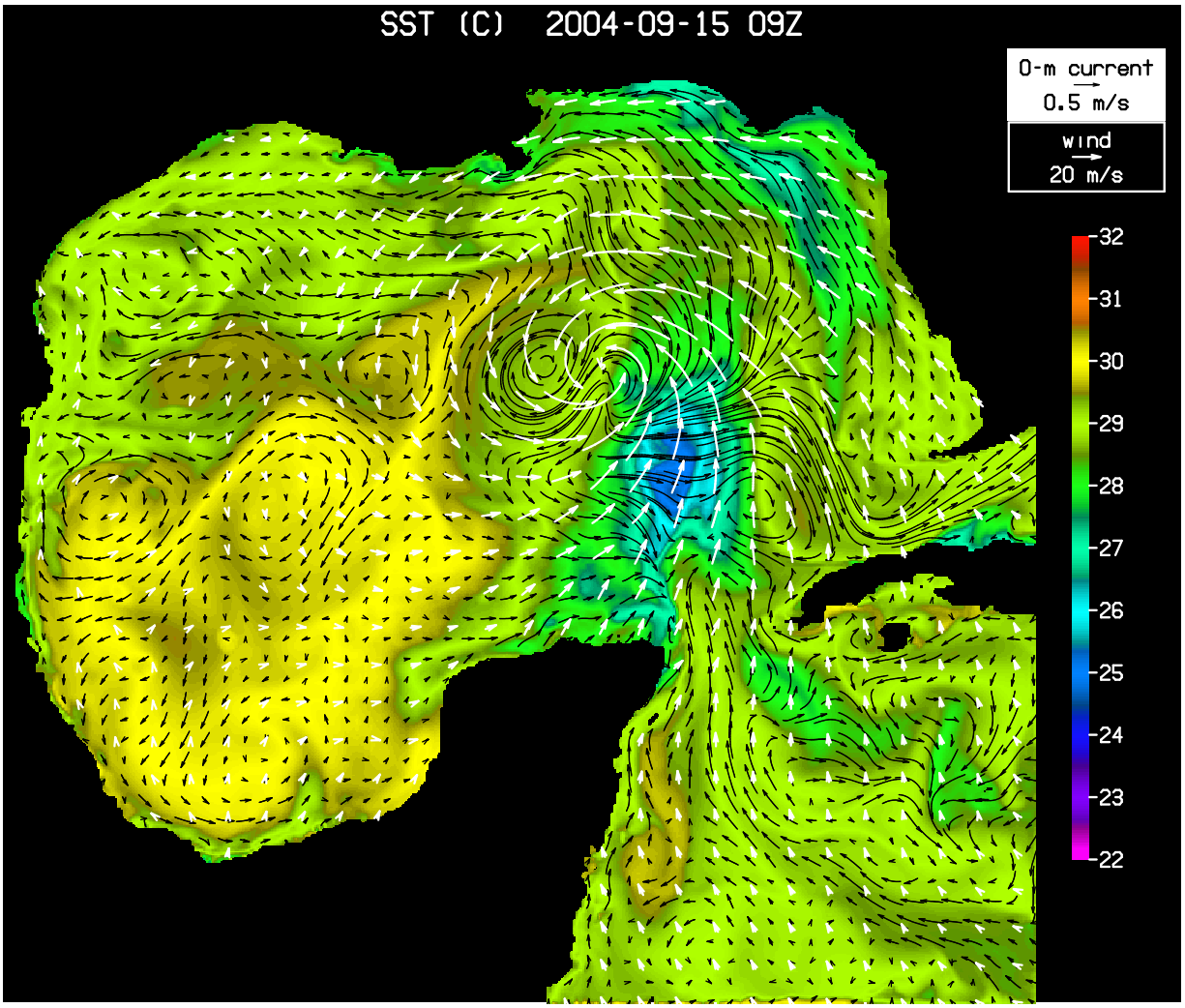

Fig. 14 — SST (color contours), SSV (black vectors), and surface winds (white vectors) at 09Z September 15, 2004 for simulation of Hurricane Ivan with the KC04 mixing enhancement

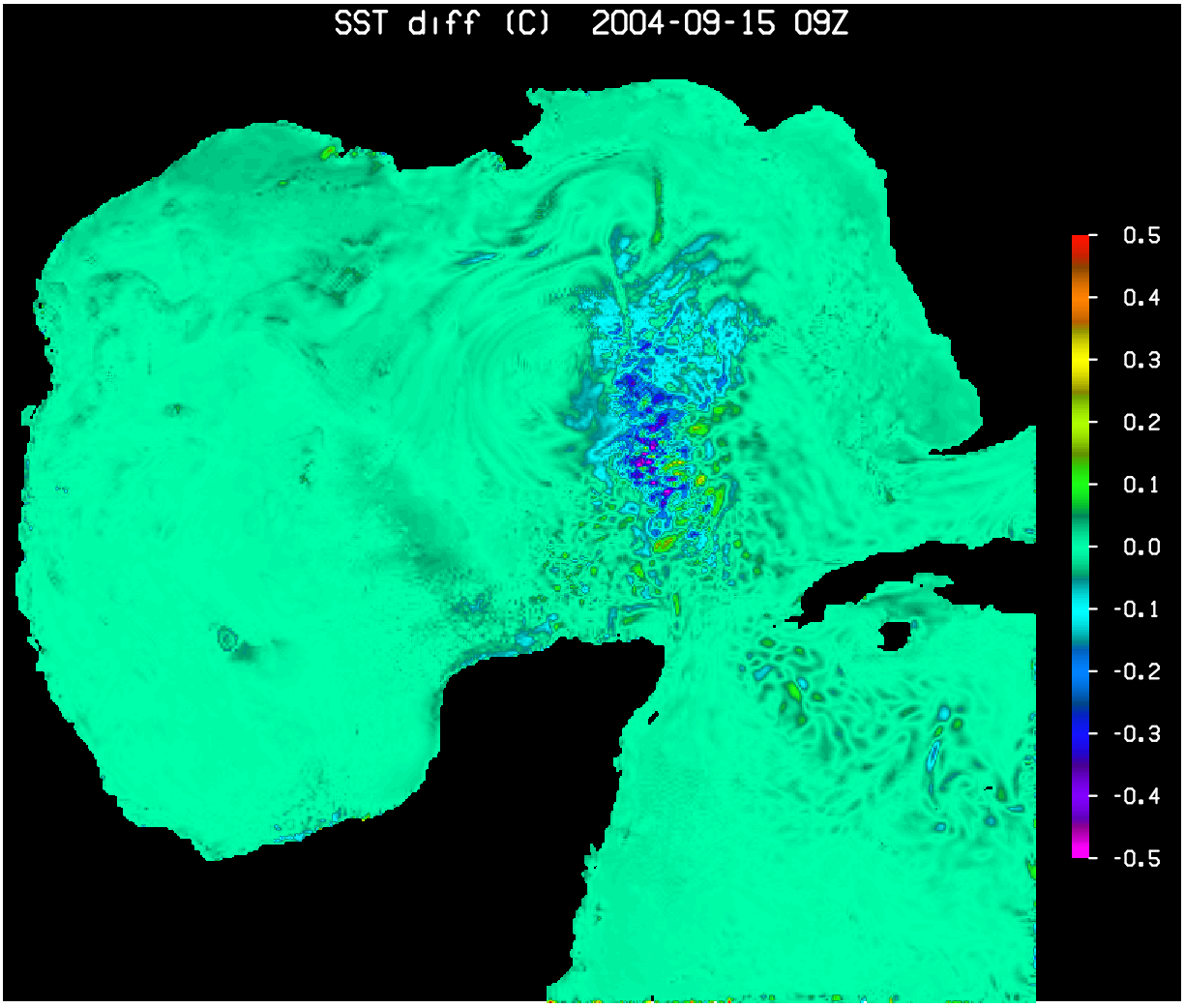

Fig. 15 — Difference in SST for Hurricane Ivan simulations with and without the KC04 mixing enhancement at 09Z September 15, 2004.

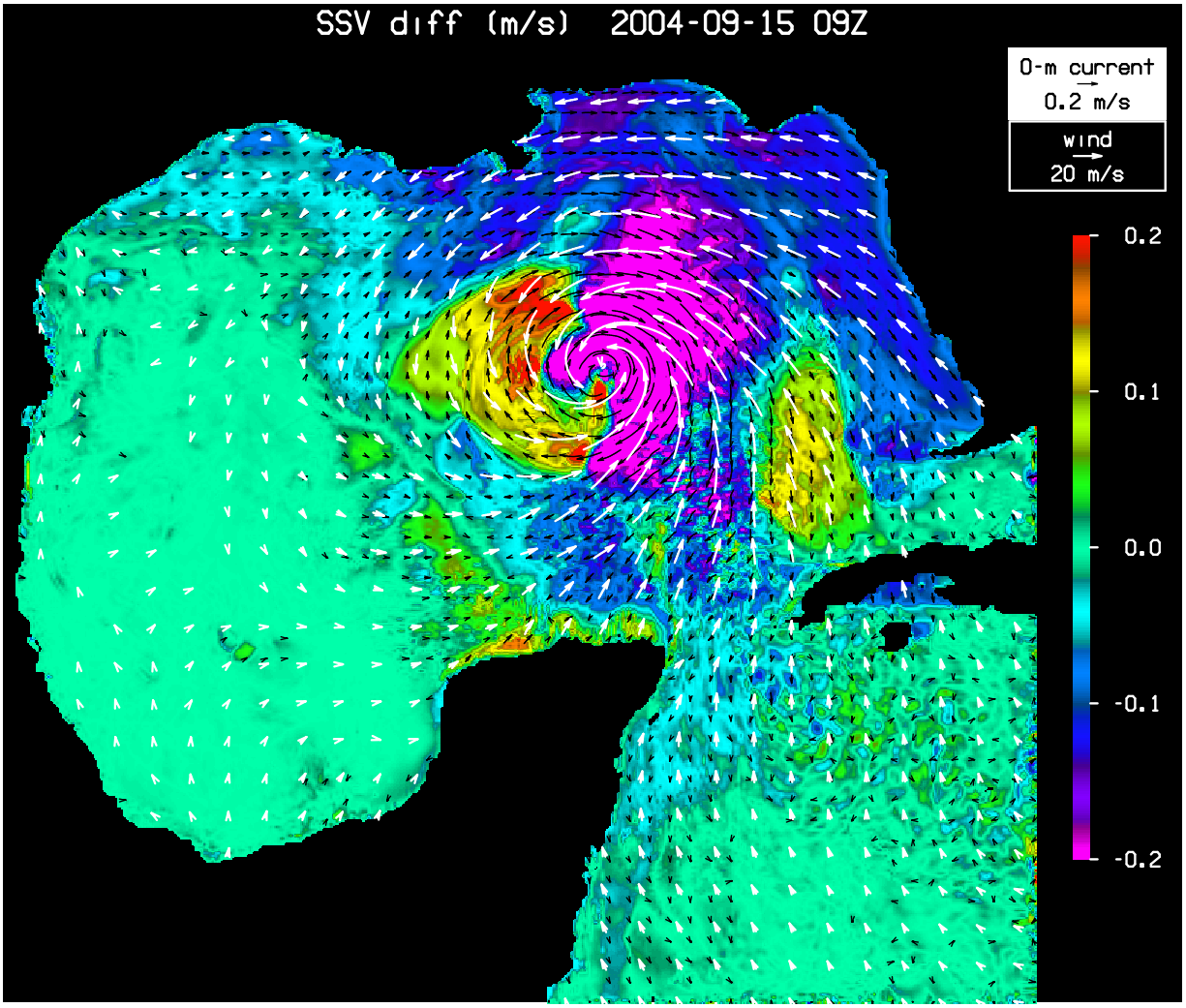

Fig. 16 — Difference in SSV for Hurricane Ivan simulations with and without the KC04 mixing enhancement at 09Z September 15, 2004. The color contours show the difference in the magnitude of the surface current and the black vectors show the vector velocity difference. The white vectors show the surface winds.

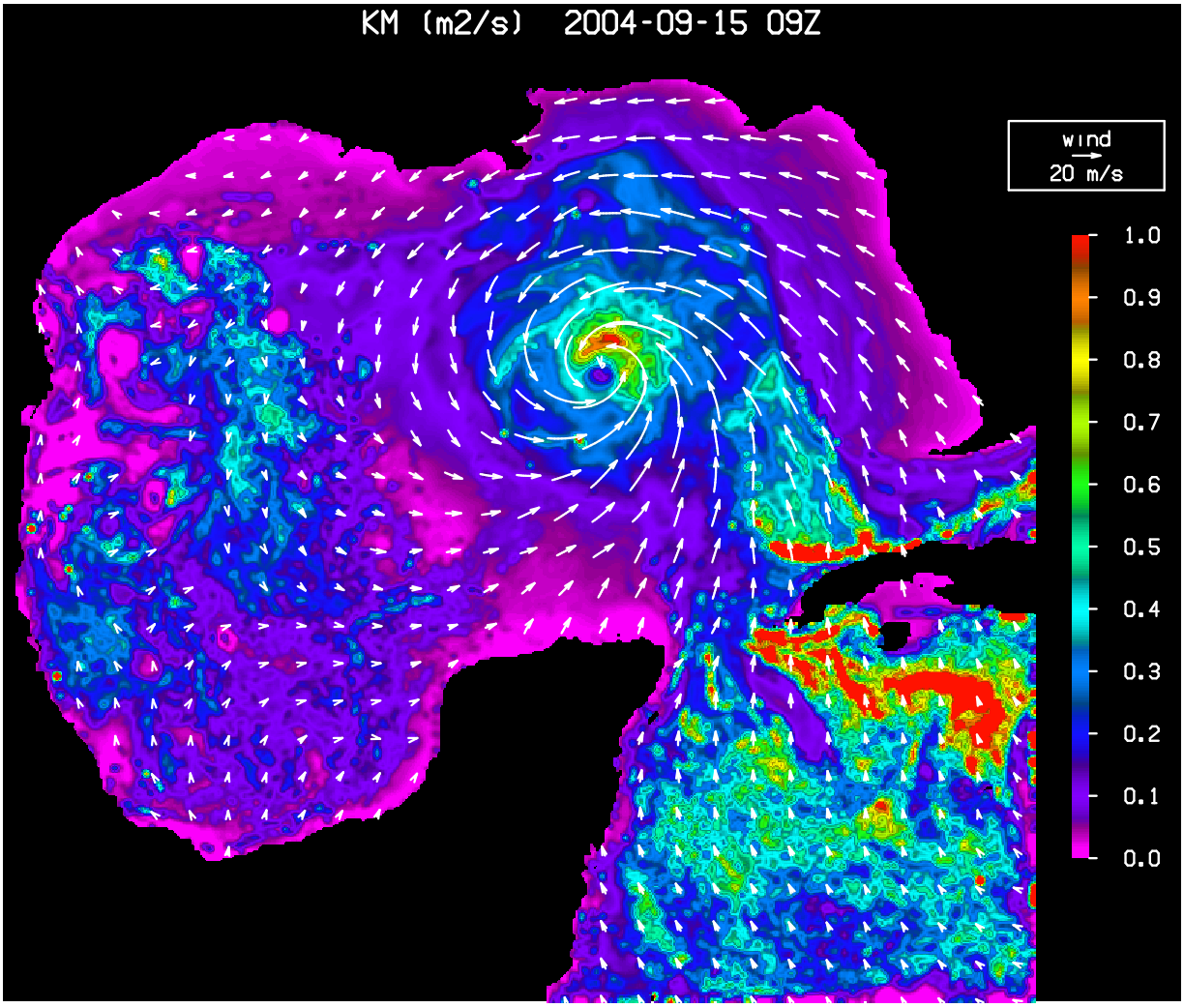

Fig. 17 — Maximum value of K_M in SML for Hurricane Ivan simulations with KC04 mixing enhancement at 09Z September 15, 2004. The white vectors show the surface winds.

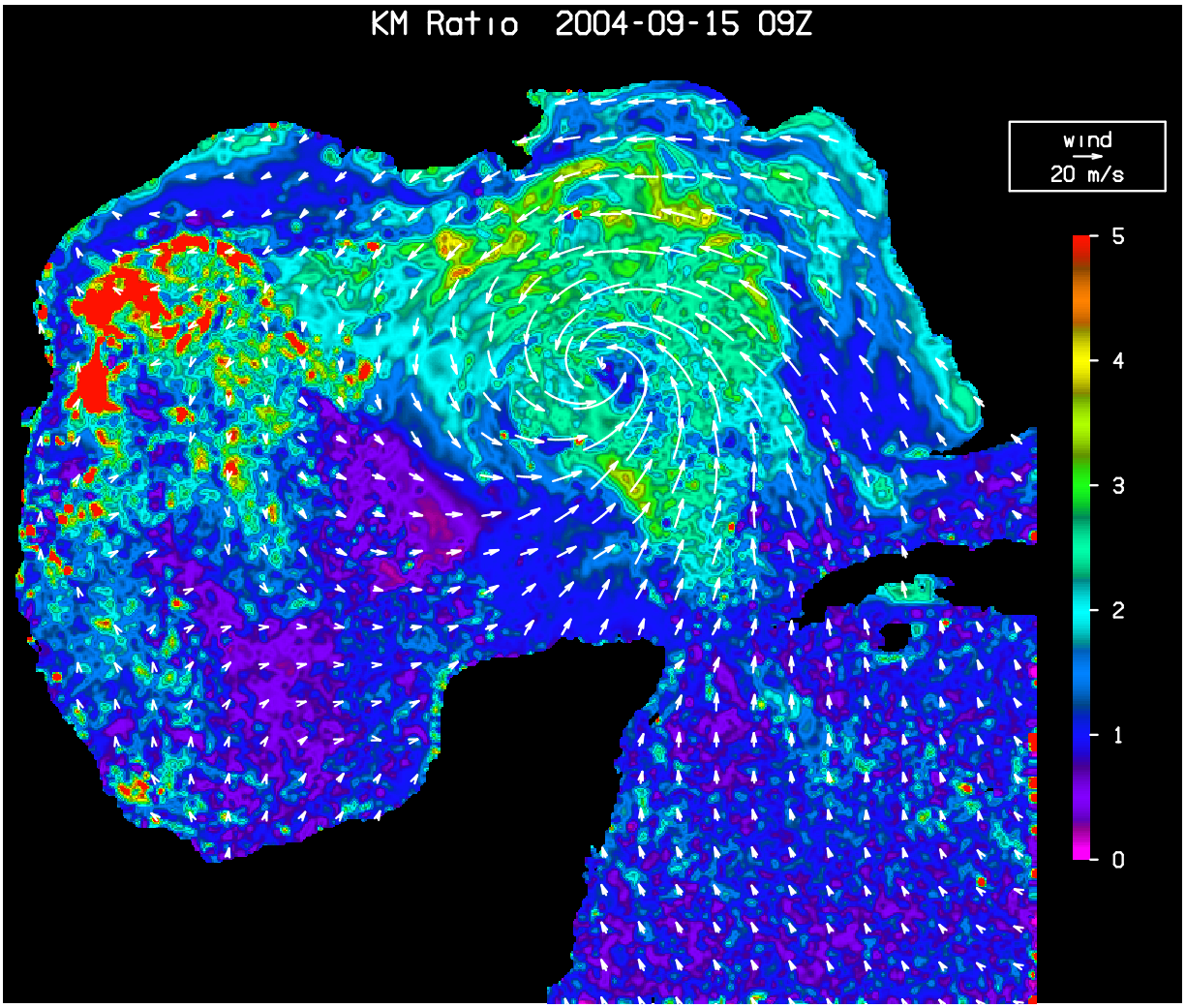

Fig. 18 — Ratio of maximum values of K_M in SML for Hurricane Ivan simulations with and without the KC04 mixing enhancement at 09Z September 15, 2004. The white vectors show the surface winds.

Figure 18 shows the ratio of the spatially-filtered values of the maximum value of K_M in the SML for the simulations with and without the the KC04 mixing enhancement at 09Z September 15, 2004. Near the hurricane, the ratios range from 1 to 4 and are frequently in the range of 2 to 3. This indicates that the KC04 scheme is significantly enhancing the mixing rates in the areas of strong hurricane winds. The areas where the ratio is below one are generally occurring in areas of night-time convection.

6. SUMMARY

Mellor-Yamada-type turbulence models have long been criticised for not mixing the ocean's surface layer strongly or deeply enough in the open ocean. Recent LES simulations of Langmuir

circulation in the upper ocean, e.g., MW97, found that the occurrence of LCs significantly increases the net rate of mixing within the SML and slightly increases the MLD. Mellor-Yamada-type turbulence models do not currently account for the effect of LCs; hence, based on the LES results of MY97, KC04 parameterized and tested the effects of LC mixing in the frequently used MYL2.5 turbulence model.

KC04 parameterized the effect of LC mixing in the MYL2.5 turbulence model by adding additional shear-production terms to the TKE and TLS equations of the turbulence model. These additional terms consist of the product of the vertical turbulent momentum flux and the vertical shear of the SDC from the surface wave field.

The KCO4 LC mixing parameterization was implemented in the MYL2.5 turbulence model in NCOM and tested by conducting simulations of the simple, light-wind, mixing case used by both MW97 and KC04, the upper-ocean thermal structure at OWS Papa during 1961, which was also used by KC04, and Hurrican Ivan in the Gulf of Mexico in 2004.

Our initial implementation of the KC04 LC mixing parameterization did not perform as well as reported by KC04, and this turned out to be due to an error in the value of the constant used to scale the SDC shear-production term in the TLS equation. The value of the constant had been incorrectly reported in the KC04 paper as 4.0, and we were advised by Dr. Lakshmi Kantha (personal communication) that it should have a value of 7.2.

Our simulation of the simple test case used by MW97 and KC04, which consists of a constant surface wind stress of 0.037 Pa (which corresponds to a wind speed of about 5 m/s) and an initial MLD of 33 m, gave results similar to those reported by both MW97 and KC04. The addition of the KC04 LC mixing parameterization increased the rate of mixing by about a factor of two and increased the MLD by about 3 m. MW97 actually showed an increase in the rate of mixing of about a factor of three, but the maximum mixing rate in the SML for all three simulations with the LC mixing was similar, i.e., about 400 m^2/s.

For the Papa simulations for 1961, no wave observations are available. Hence, we used three methods to estimate the SDC: (1) the parameterization of the SDC in terms of the surface friction velocity u_* used by KC04 in their tests at Papa, (2) the calculation of the mean wave-energy spectrum at different wind speeds using data from NOAA Buoy 46005 in the northeast Pacific, and (3) the waves predicted by the SWAN wave model, which was run using the observed winds at Papa for 1961.

For all three calculations of the SDC at Papa, the use of the KC04 LC mixing parameterization significantly increased the rate of mixing within the SML and increased the MLD. However, the methods (1) to (3) of computing the SDC yielded sucessively smaller values of the SDC, at least during the heating season in the spring and summer, which resulted in slightly reduced mixing rates and reduced deepening of the SML. The mean rate of mixing within the SML in the spring and summer was increased by a factor of about 2 for methods (1) and (2) and by a factor of about 1.4 for method (3). Note that for method (1), KC04 indicated that the scaling parameter they used to compute the SDC from u_* was on the high side; hence, the fact that the SDCs computed in this way for OWS Papa for 1961 are significantly higher than the SWAN SDCs suggests that this is the case.

The use of the KC04 LC mixing parameterization, besides increasing the rate of mixing within the SML, also increases the MLD. However, for the basic MYL2.5 turbulence model, the increase in the MLD provided by the KC04 LC mixing parameterization is not deep enough to match the observed MLD at Papa for 1961. Hence, it may be that an additional mechanism is needed to provide the needed additional deepening, e.g., the parameterization of intermittent mixing below the SML (e.g., by internal waves) of Large et al. (1994).

The additional shear-production terms in the TKE and TLS equations implemented by KC04, which consist of the product of the vertical momentum flux and the vertical shear of the SDC, can make a negative contribution to the total shear production of TKE if the vertical shear of the ocean model velocity and the vertical shear of the SDC are of opposite sign. The fact that mixing rates with the KC04 mixing enhancement are sometimes less than without it suggests that this sometimes occurs. A simulation was conducted at Papa with the SWAN SDC with KC04's SDC-shear-production terms in the TKE and TLS equations forced to make a positive contribution to the total shear production of TKE by using their absolute value. The result was that the occurrence of reduced mixing rates when using the KC04 LC mixing parameterization was reduced, and the ratio of the mean value of the vertical mixing coefficients during the spring and summer for the cases with and without the LC-mixing parameterization was increased slightly from 1.4 to 1.6.

In computing the SDC at Papa using methods (1) and (2), the SDC was taken to be in the same direction as the wind. However, the waves predicted by SWAN in method (3) (and, of course, real waves) often propagate in a direction different from that of the wind, and waves of different wavelengths may propagate in different directions, which results in a change in direction of the SDC with depth. The effect of this on the contribution to the vertical mixing from the KC04 LC mixing parameterization was investigated by conducting a simulation at Papa with the SWAN SDC modified to always be alligned with the wind. The effect of this change on the simulation was small, i.e., the SST, MLD, and mixing rates within the SML were not much affected.

For the simulations of Hurrican Ivan in the Gulf of Mexico, the use of the KC04 LC mixing parameterization generally results in significantly increased mixing rates in the SML near the hurricane, i.e., the mixing rates are frequently increased by a factor of 2 to 3. The increased mixing rates result in a significant reduction in the vertical shear of the wind-driven currents in the SML, which results in a reduction of the surface value of the wind-driven current near the hurricane of 20 cm/s or more. The depth of mixing is also slightly increased, which results in increased cooling of the SST, though this additional SST cooling is small, i.e., generally less than 0.5 °C.

7. ACKNOWLEDGMENTS

Thanks to Dr. Lakshmi Kantha for helpful discussions regarding the implementation of his parameterization of Langmuir circulation mixing in the Mellor-Yamada Level 2.5 turbulence model. This work was funded through the 6.2 NRL Core Project "Coupled Ocean-Wave Prediction System," and through the 6.2 NRL Core Project "Full Column Mixing for Numerical Ocean Models."

8. REFERENCES

Barron, C.N., A.B. Kara, H.E. Hurlburt, C. Rowley, and L.F. Smedstad (2004). "Sea Surface Height Predictions from the Global Navy Coastal Ocean Model (NCOM) During 1998–2001," *J. Atmos. Oceanic Technol.* **21**(12), 1876–1894.

Bidlot, J.-R., D.J. Holmes, P.A. Wittmann, R. Lalbeharry, and H.S. Chen (2002). "Intercomparison of the Performance of Operational Ocean Wave Forecasting Systems with Buoy Data," *Wea. Forecasting* **17**, 287-310.

Booij, N., R.C. Ris, and L.H. Holthuijsen (1999). "A Third-Generation Wave Model for Coastal Regions: 1. Model Description and Validation," *J. Geophys. Res.* **104**(C4), 7649–7666.

Charnock, H. (1955). "Wind Stress on a Water Surface," *Quart. J. Roy. Meteor. Soc.* **81**, 639–640.

Craig, P.D. and M.L. Banner (1994). "Modeling Wave-enhanced Turbulence in the Ocean Surface Layer," *J. Phys. Oceanogr.* **24**, 2546–2559.

Denman, K.L. and M. Miyake (1973). "Upper Layer Modification at Ocean Station Papa: Observations and Simulation," *J. Phys. Oceanogr.* **3**, 185–196.

Gaspar, P. (1988). "Modeling the Seasonal Cycle of the Upper Ocean," *J. Phys. Oceanogr.* **18**, 161–180.

Grant, W.D. and O.S. Madsen (1979). "Combined Wave and Current Interaction with a Rough Bottom," *J. Geophys. Res.* **84**, 1979–1808.

Hodur, R.M. (1997). "The Naval Research Laboratory's Coupled Ocean/Atmosphere Mesoscale Prediction System (COAMPS)," *Mon. Wea. Rev.* **125**, 1414–1430.

Jerlov, N. G. (1968). *Optical Oceanography* (Elsevier Publ. Co., Inc., New York), 194 pp.

Kantha L.H. and C.A. Clayson (1994). "An Improved Mixed Layer Model for Geophysical Applications," *J. Geophys. Res.* **99**, 25235–25266.

Kantha L.H. and C.A. Clayson (2004). "On the Effect of Surface Gravity Waves on Mixing in the Oceanic Mixed Layer," *Ocean Modelling* **6**, 101–124.

Komen, G.J., S. Hasselmann, and K. Hasselmann (1984). "On the Existence of a Fully Developed Wind-Sea Spectrum," *J. Phys. Oceanogr.* **14**, 1271–1285.

Large, W.G. (1996). "An Observational and Numerical Investigation of the Climatological Heat and Salt Balances at OWS Papa," *J. Climate* **9**, 1856–1876.

Large, W.G., J.C. McWilliams, and S. Doney (1994). "Oceanic Vertical Mixing: a Review and a Model with a Nonlocal Boundary Layer Parameterization," *Rev. Geophys.* **32**, 363–403.

Levitus, S. (1982). "Climatological Atlas of the World Ocean," NOAA Prof. Paper 13, U.S. Govt. Print Office, Washington, D.C., 173 pp.

Li, M., C. Garrett, and E. Skyllingstad (2005). "A Regime Diagram for Classifying Turbulent Large Eddies in the Upper Ocean," *Deep-Sea Res.* **52**, 259–278.

Martin, P. J. (1982). "Mixed-Layer Simulation of Buoy Observations Taken During Hurricane Eloise." *J. Geophys. Res.* **87**, 409–427.

Martin, P. J. (1985). "Simulation of the Mixed Layer at OWS N and P with Several Models," *J. Geophys. Res.* **90**, 903–916.

Martin, P. J. (1986). "Testing and Comparison of Several Mixed-Layer Models," NORDA Report 143. Naval Research Laboratory, Stennis Space Center, MS 39529, 30 pp.

Martin, P.J. (2000). "A Description of the Navy Coastal Ocean Model Version 1.0," NRL Report NRL/FR/7322–00-9962, Naval Research Laboratory, SSC, MS 39529, 42 pp.

Martin, P.J., E. Rogers, R.A. Allard, P.J. Hogan, and J.G. Richman (2012). "Results from Tests of Direct Wave Mixing in the Ocean's Surface Mixed Layer." NRL Report NRL/FR/7322–12-10216, Naval Research Laboratory, SSC, MS 39529, 35 pp.

McWilliams, J.C., P.P. Sullivan, and C.-H. Moeng (1997). "Langmuir Turbulence in the Ocean." *J. Fluid Mech.* **334**, 1–30.

Mellor, G.L. and A. Blumberg (2004). "Wave Breaking and Ocean Surface Layer Thermal Response." *J. Phys. Oceanogr.* **34**, 693–698.

Mellor, G.L. and P.A. Durbin (1975). "The Structure and Dynamics of the Ocean Surface Mixed Layer," *J. Phys. Oceanogr.* **5**, 718–728.

Mellor, G.L. and T. Yamada (1974). "A Hierarchy of Turbulence Closure Models for Planetary Boundary Layers," *J. Atmos. Sci.* **31**, 1791–1806.

Mellor, G.L. and T. Yamada (1982). "Development of a Turbulence Closure Model for Geophysical Fluid Problems," *Geophys. and Space Phys.* **20**, 851–875.

Morey, S.L., P.J. Martin, J.J. O'Brien, A.A. Wallcraft, and J. Zavala-Hidalgo (2003). "Export Pathways for River Discharged Fresh Water in the Northern Gulf of Mexico," *J. Geophys. Res.*, **108**, 1–15.

Price, J.F. (1981). "On the Upper-Ocean Response to a Moving Hurricane," *J. Phys. Oceanogr.* **11**, 153–175.

Rosmond, T.E., J. Teixeira, M. Peng, T.F. Hogan, and R. Pauley (2002), "Navy Operational Global Atmospheric Prediction System (NOGAPS): Forcing for Ocean Models," *Oceanography* **15**, 99–108.

Skyllingstad, E.D., and D.W. Denbo (1995). "An Ocean Large-Eddy Simulation of Langmuir Circulations and Convection in the Surface Mixed Layer," *J. Geophys. Res.* **100**, 8501–8522.

Soulsby, R.L. (1995). "Bed Shear-Stresses Due to Combined Waves and Currents," in *Advances in Coastal Morphodynamics*, edited by M. Stive, J. Fredsoe, L. Hamm, R. Soulsby, C. Teisson, and J. Winterwerp, Delft Hydraulics, Delft, The Netherlands, 420–423.

Wu, J. (1980). "Wind-Stress Coefficients Over Sea Surface Near Neutral Conditions," *J. Phys. Oceanogr.* **10**, 727–740.

Appendix A

CALCULATION OF SDC FOR A MONOCROMATIC WAVE

The Stokes drift current (SDC) V_s can be computed for a monocromatic (i.e., single frequency) wave using

$$V_s(z) = (ak)^2 c_p \frac{\cosh(2k(H+z))}{2\sinh^2(kH)}, \tag{A1}$$

where a is the wave amplitude, $k = 2\pi/L$ is the wavenumber, L is the wavelength, $c_p = (\tanh(kH)g/k)^{\frac{1}{2}}$ is the phase speed, g is the acceleration of gravity, H is the total water depth, and z is the distance to the surface.

In deep water, this simplifies to

$$V_s(z) = (ak)^2 c_p \exp(2kz), \tag{A2}$$

where the phase speed is $c_p = (g/k)^{\frac{1}{2}}$.

For a wave field consisting of waves of different amplitudes, frequencies, and directions, the contributions to the SDC from the different waves can be summed (in a vector sense).

The wave amplitude a is related to the wave energy E as

$$E = \frac{1}{2}a^2. \tag{A3}$$

Note that the wave energy given by Eq. (A3) has units of length squared, which is a common practice when discussing surface waves. Multiplication by the water density and the acceleration of gravity gives the proper units of energy per m^2 of surface area.

Appendix B

CALCULATION OF SDC FROM WIND STRESS BY KC04

Kantha and Clayson (2004) estimated the surface value of the SDC $V_s(z=0)$ in deep water using

$$V_s(z=0) = 11.8u_*, \tag{B1}$$

where $u_* = (\tau/\rho_w)^{\frac{1}{2}}$ is the water-side surface friction velocity, τ is the surface wind stress, and ρ_w is the water density. The wavenumber k associated with the peak of the wave energy spectrum is parameterized as

$$k = 4.05 \times 10^{-6} g/u_*^2. \tag{B2}$$

Hence, the SDC profile is given by

$$V_s(z) = 11.8u_* exp(2kz), \tag{B3}$$

with k given by Eq. B2.

Appendix C

CALCULATION OF SDC USING WAVE SPECTRA FROM NOAA BUOY

Some of the NOAA buoys provide observations of both the surface wind velocity and the wave energy spectra. These data allow the calculation of the average wave spectra at different wind speeds. The average wave spectra at the different wind speeds can then be used to estimate the SDC for a given wind speed.

The spectral wind and wave data that were used were from NOAA Buoy 46005, which is located in the northeast Pacific at 131.001 °W, 46.100 °N, which is about 1100 km east-southeast of the location of OWS Papa. Since the location of the buoy is somewhat similar to that of OWS Papa, the wind and wave conditions should be roughly similar.

Data from Buoy 46005 for the years 1996 through 2004 were used. For these years, the spectral wave data from the buoy consist of 38 values of the wave energy at frequencies from 0.03 to 0.4 Hz at 0.01 Hz intervals. Note that no directional information is provided for the wave data from Buoy 46005. Averages of the spectral data were computed within 1-m/s-wide wind-speed bins from 1 to 20 m/s. No winds above 20 m/s were recorded at Buoy 46005 during the 9-year period. The wind speed used to characterize the wave spectrum in this calculation is the wind speed at the time of the wave observation. An alternative would be to use some time-weighted wind speed over the previous few hours, but this was not done.

Figure C1 shows the averaged wave spectra from NOAA Buoy 46005 for wind speeds of 1, 5, 10, 15, and 20 m/s. The wave energy increases with increasing wind speed. There are, however, a couple of notable aspects to the wave spectra in Fig. C1: (1) the location of the peak of the wave energy spectra shows little change with wind speed, and (2) there is a notable amount of wave energy present at low wind speeds of 1 to 5 m/s.

There are several limitations to estimating the SDC from a wave spectra based on the current local wind velocity. The wind duration and fetch and the propagation of waves from other areas cannot be accounted for. Additionally, variation in the direction of the waves making up the energy spectrum cannot be accounted for; hence, the direction of the waves and the SDC is assumed to be downwind.

The SDC profiles estimated from the wave spectra at Buoy 46005 for different wind speeds were compared with the SDC profiles computed from the observed wave spectra using data for the year 2000, and the mean and rms differences versus depth are shown in Fig. C2. The SDC estimated by this method will be referred to as the Buoy Wave Spectra (BWS) SDC. Mean and RMS errors with respect to the SDC computed from the buoy wave observations for 2000 are also shown for the SDC computed using the KC04 method discussed in Appendix C2.

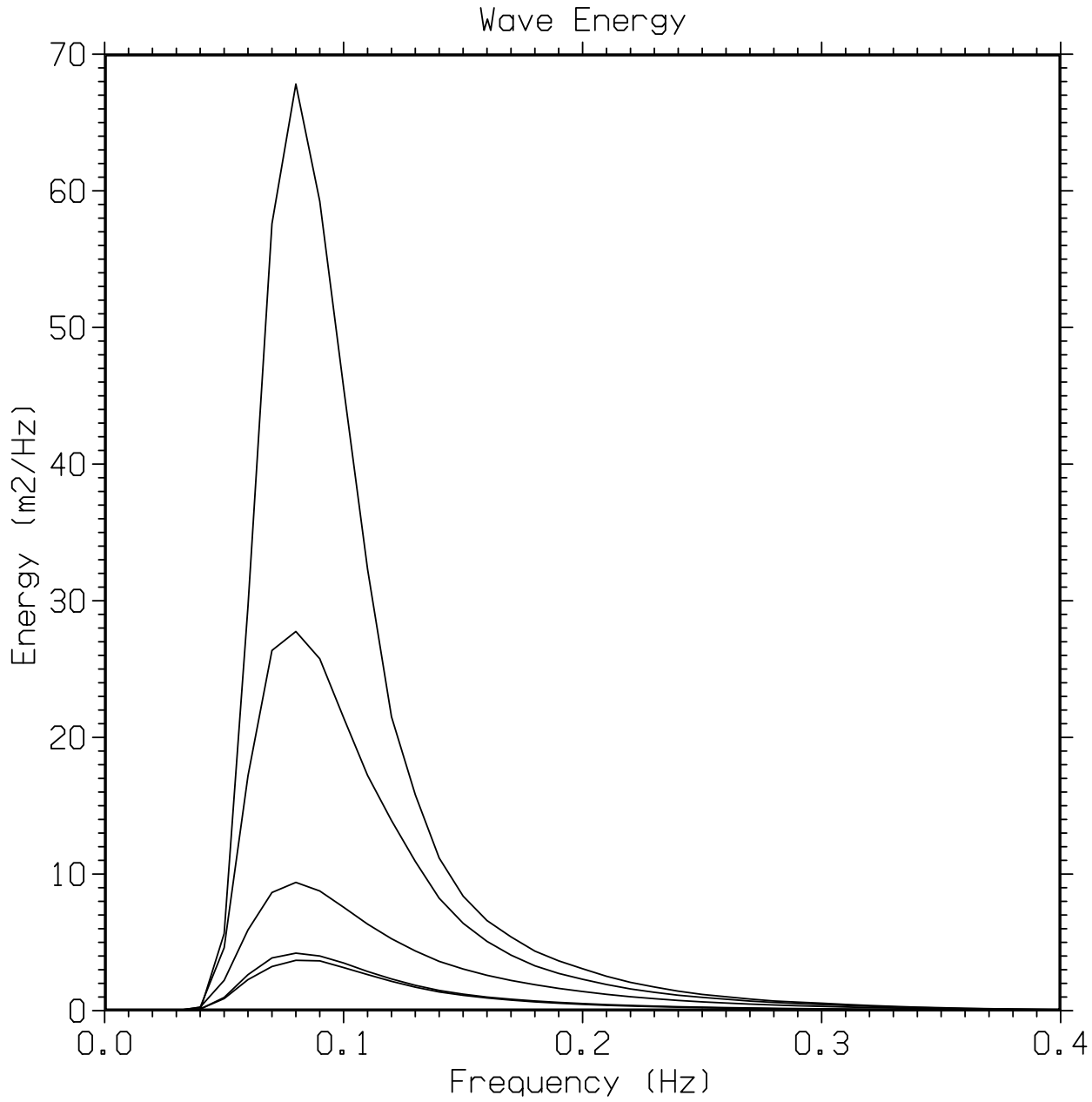

Fig. C1 — Averaged wave spectra from NOAA Buoy 46005 for wind speeds of 1, 5, 10, 15, and 20 m/s. The wave energy increases with wind speed.

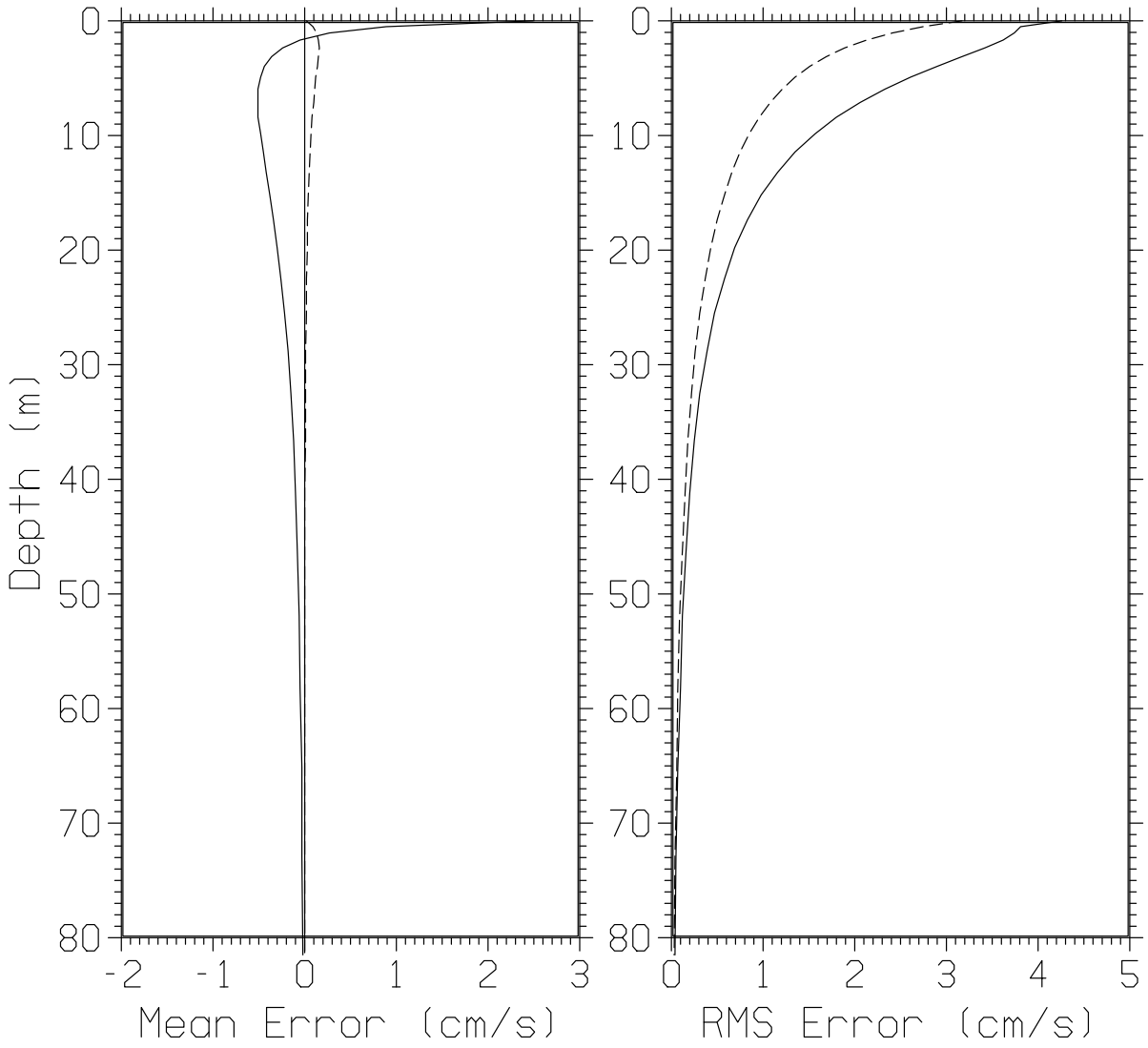

Fig. C2 — Mean and RMS error for the KC04-computed (solid line) and BWS-computed (dashed line) SDC at buoy 46005 for the year 2000. Errors are with respect to the SDC computed from the observed wave spectra at buoy 46005 for the year 2000.

Figure C2 shows that both the mean and RMS errors are noticeably smaller for the BWS SDC than for the SDC estimated using the method of KC04. Plots for the same errors computed using data from buoy 46005 for other years between 1996 and 2004 (not shown) look similar to Fig.C2.

Appendix D

CALCULATION OF SDC WITH SWAN WAVE MODEL

This section discusses the use of the SWAN wave model (Booij et al. 1999) to estimate the wave spectra and SDC at OWS Papa. For the application of SWAN at a single location, the geographic advection terms and a feature known as "quadrant sweeping" are disabled. The use of a wave model at a single location allows accounting for the recent time history of the local winds, including changes in both magnitude and direction. However, it does not allow a proper accounting for swell from other areas, where the winds are likely to be different.

Rather than apply the model with the Papa winds blindly, we first perform several experiments for a situation where simultaneous observations of wind speed and wave spectra are available, i.e., with the data from NOAA buoy 46005 during the year 2000. As noted previously, buoy 46005 is located about 1100 km east-southeast of the location of OWS Papa, so the winds should be roughly similar in a statistical sense. With the buoy data, we can check the accuracy of our method, and evaluate simulations with several, alternative, wave-model source-term settings. To simplify the analysis of the results, we look at the significant wave height (SWH) only, rather than the wave spectra. (An alternative would be to look at an omni-directional calculation of the Stokes drift at a selected depth.)

The physics packages available with the version of SWAN that we have that are compared here are: (1) the Komen et al. (1984) physics (denoted here as KHH, this is the SWAN default) with the Wu (1980) drag formulation, (2) the KHH physics with modification according to Rogers et al. (2003) with the Hwang (2011) drag formulation, (3) the Rogers et al. (2012) physics (denoted as RBW) with the Hwang (2011) drag formulation without swell dissipation, and (4) variants of (3) with the swell dissipation strength controlled by the swell dissipation coefficient fe. For further description of these physics packages, the reader is referred to Rogers et al. (2012).

The duration of the test simulations is one year. The mean and rms errors for the SWH for the tests that were run are listed in Table D1. Errors for the previous KC04 and BWS parameterizations of the wave field in terms of the local winds are also provided in Table D1 for comparison.

The minimum error in Table D1 is for the SWAN simulation with the Rogers et al. (2012) physics with the Hwang (2011) drag formulation with a swell dissipation coefficient of 0.003. The SWH RMS error for this simulation is 0.99 m. Figure D1 shows a scatter plot of the SWH predicted by SWAN for this case versus the observed SWH at buoy 46005 during the year 2000.

Though the SWH RMS error of 0.99 m is the lowest that was obtained in the tests conducted with the buoy data, this is significantly greater than the SWH RMS error of 0.4 to 0.6 m typically expected for global wave hindcasts (e.g., Bidlot et al. 2002). This larger error for the wave simulation at buoy 46005 can be blamed on the use of a single-point wave model, which has these limitations:

Table D1 — Significant Wave Height Errors Using Data From Buoy 46005

model	*physics*	*bias error* (m)	*rms error* (m)
SWAN	KHH/Wu, $n = 1$	-1.09	1.43
SWAN	KHH/Hwang, $n = 2$	2.16	2.37
SWAN	RBW, $fe = 0.000$	9.58	9.81
SWAN	RBW, $fe = 0.002$	0.51	1.20
SWAN	RBW, $fe = 0.003$	-0.03	0.99
SWAN	RBW, $fe = 0.004$	-0.34	1.00
SWAN	RBW, $fe = 0.005$	-0.69	1.16
KC04		-1.20	1.74
BWS		0.28	1.13

(1) it assumes uniform winds within an infinite ocean domain, i.e., the fetch is effectively infinite, (2) it cannot use advection to remove swell energy, the energy can be removed only via dissipation, and (3) it cannot use advection to bring in swell energy, energy is created only via the wind input physics,

Intuition tells us that a single-point wave model will tend to do best during periods when the sea state is dominated by local winds. Further, it is intuitive that models with weak swell dissipation, e.g., the SWAN simulations with the KHH/Hwang physics with $n = 2$ and with the RBW physics with $fe = 0$, will tend to perform poorly.

Based on these results, the SWAN wave model with the RBW physics with $fe = 0.003$ is applied to the Papa wind data set to estimate the wave spectra and, from the wave spectra, the Stokes drift.

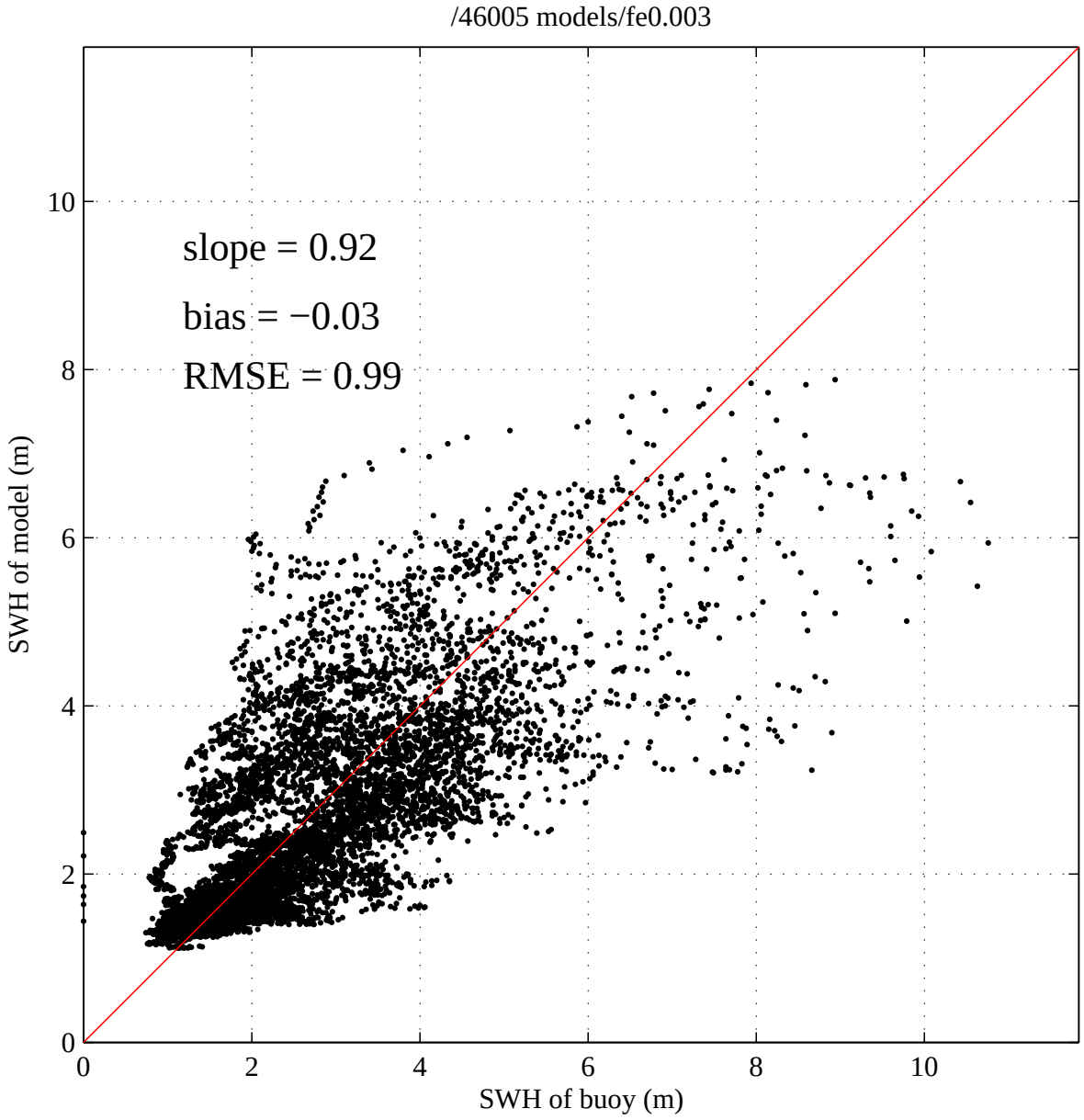

Fig. D1 — Scatter plot of SWH predicted by SWAN versus observed SWH at Buoy 46005 for year 2000 for SWAN simulation with minimum error, i.e., with RBW physics with fe = 0.003.